

See discussions, stats, and author profiles for this publication at: <https://www.researchgate.net/publication/259667795>

A Finite Cluster Approach to an Extended Transition Metal Oxide: A Wave Function Based Study

ARTICLE *in* THE JOURNAL OF PHYSICAL CHEMISTRY C · AUGUST 2011

Impact Factor: 4.77 · DOI: 10.1021/jp203654m

CITATIONS

6

READS

30

2 AUTHORS, INCLUDING:



Maria Pilar De Lara-Castells

Spanish National Research Council

72 PUBLICATIONS 726 CITATIONS

[SEE PROFILE](#)

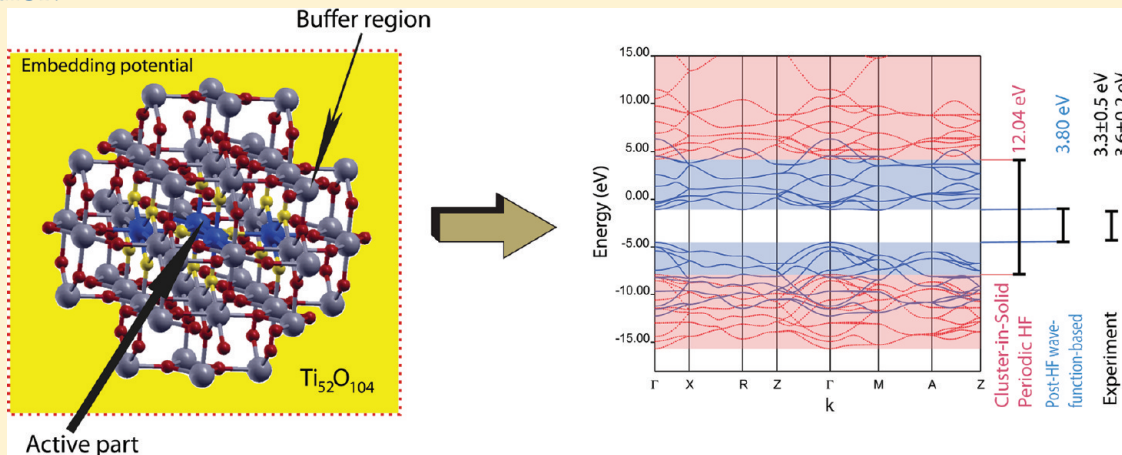
A Finite Cluster Approach to an Extended Transition Metal Oxide: A Wave Function Based Study

María Pilar de Lara-Castells*

Instituto de Física Fundamental (C.S.I.C.), Serrano 123, E-28006, Madrid, Spain

Alexander O. Mitrushchenkov[§]

Université Paris-Est, Laboratoire Modélisation et Simulation Multi Echelle, MSME UMR 8208 CNRS, 5 bd Descartes, 77454 Marne-la-Vallée, France

^S Supporting Information**ABSTRACT:**

An accurate finite cluster approach based on localized Wannier orbitals is applied here to bulk TiO_2 as a prototypical extended transition metal oxide. The quasi-particle band structure, an extended property of the infinite solid, is successfully reproduced within a finite local cluster approach at the Hartree–Fock level. Post-Hartree–Fock calculations on selected clusters are then performed to account for correlation effects. The computational implementation, which is a modified version of the “cluster-in-solid” embedding technique (Birkenheuer, U., Fulde, P.; Stoll, H. *Theor. Chem. Acc.* 2006, 116, 398) along with the frozen local hole approximation (Pahl, E.; Birkenheuer, U. *J. Chem. Phys.* 2006, 124 214101), is described and possible further extensions to calculate local defects in bulk materials and excited states in adsorbate/metal oxide surfaces are discussed.

I. INTRODUCTION

First-principle studies of excited states on extended (semiconductor) metal oxides are required for understanding their photocatalytic properties, which are important in the development of novel materials for cost-effective solar energy technologies or in solar-powered environmental remediation.^{1,2} However, due mainly to the complexity of the quantum treatment of excited states in extended systems, ab initio surface photochemistry studies are still scarce.^{3–5} In fact, standard current computational methodology for two- and three-dimensional periodic systems is normally restricted to the application of Hartree–Fock (HF), density functional theory (DFT), or hybrid HF/DFT-type approaches. In general, though, HF provides a poor description of excited states energies and conventional DFT is formally a ground-state theory. Although some dynamic

correlation methods were recently implemented, such as second-order Möller–Plesset perturbational schemes⁶ and (in the particular case of one-dimensional systems) those based on the coupled-cluster (CC) theory,⁷ they are still limited to periodic conditions. On the other hand, standard quantum-chemistry molecular codes have a rich tool box of different methods to accurately treat both dynamic correlation and complicated multi-reference or open-shell cases often occurring in excited states. These methods, however, are restricted to finite molecules (clusters) and cannot deal with an infinite periodic environment.

Received: April 19, 2011**Revised:** July 25, 2011**Published:** August 01, 2011

In the particular case of excited states of molecules adsorbed on metal oxide surfaces, model (finite) cluster approaches (i.e., embedded in a semi-infinite Madelung potential of point charges or by employing hydrogen atoms to saturate the dangling bonds at their ends) have been found to be very useful when describing excitations localized within a finite region of the adsorbate–substrate complex^{3,5} and, therefore, highly correlated methods used for molecular systems can be applied to calculate not only total energies but also the dipole-induced and electronic couplings between the interacting electronic states. When the involved excited states have a charge-transfer character emerging from ionic and localized adsorbate–substrate interactions, the nonorthogonal multireference configuration interaction (MRCI) method has been shown to provide accurate dipole-moment and electronic couplings in a quasi-diabatic representation and thus probabilities for the charge transfer process.⁵ However, continuous properties such as the quasi-particle (QP) band structures are harder to reproduce within these models. On the other hand, the band structure, essentially describing excitations between N and $N \pm 1$ electron-addition (removal) states (referred to as electron (hole) states) over the extended condensed phase, is a fundamental property when considering, e.g., substrate-mediated surface photochemistry at ab initio level. This is the case for the O₂ photodesorption from a reduced titanium dioxide (110) surface, where O₂ has been used as a probe molecule to monitor the photogenerated hole and electron carriers by Yates and collaborators (see for example ref 8 and references therein). Titanium dioxide TiO₂ has wide-ranging and important applications in photoelectronics and photocatalysis,^{9–12} making it one of the most studied metal oxides. It has been found in previous experimental^{1,13–15} and theoretical^{5,16} studies that the electronic O₂ desorption is caused by the capture of holes from the bulk material. Model system bath Hamiltonian approaches, in which some parameters are fitted to either experimental or ab initio data have been specifically designed for handling the substrate-mediated electronic quenching of the excited adsorbate–substrate complex,³ with a localized region described as accurately as possible by employing state-of-the-art ab initio methods designed for molecular systems.^{3,5} It is therefore important to implement and develop methods that accurately describe continuous excited-state bulk properties and, at the same time, provide a correlated description of the primary region of the adsorbate–substrate complex.

When the interfacial charge-transfer process¹⁷ is modeled in dye-sensitized semiconductors, a unified picture of the adsorbate–substrate system was developed as the combination of state-of-the-art nonadiabatic molecular dynamics¹⁸ and time-dependent DFT¹⁹ by, e.g., Duncan and Prezhdo²⁰ and Rego and Batista.²¹ Also within the context of DFT-based methods, the embedding technique, first proposed by Wesolowski and Washell²² and later extended and adapted to deal with metal surfaces by Carter and collaborators,^{23,24} became a powerful hybrid approach in which DFT treatment of the extended system is combined consistently with a highly correlated description of the adsorbate–substrate complex by adding an external one-electron potential that accounts for infinite environment effects. However, when applied to the band structure of semiconductors and insulators, standard DFT-based methods (i.e., using the Kohn–Sham (KS) formulation and the local-density approximation (LDA)) the band gap is systematically underestimated (the so-called “band-gap problem”²⁵). There is in fact no rigorous foundation to relate the KS

eigenvalues with the electronic band structure. In contrast, Koopmans’ theorem relates the HF eigenvalues to the electronic band structure, but the neglect of correlation strongly overestimates the energy of the unoccupied (virtual) orbitals and thus the fundamental band gap. It has been shown that the systematic underestimation of the band gap in DFT can be corrected by incorporating a fraction of single-determinant exchange within the hybrid DFT/HF approaches.²⁶ Also within the framework of DFT, band structures in agreement with experiment can be obtained by employing Green’s functions techniques (e.g., using the GW approximation²⁷ for the electronic self-energy and combining it with the exchange optimized potential approach²⁸), time-dependent DFT,¹⁹ or dynamic mean field theory.²⁹ Concerning post-HF wave function based methods to introduce correlation effects in band-structure calculations, localized orbitals are usually employed where the local character of the electron correlations is exploited to render the treatment feasible. In particular, the local Hamiltonian approach (LHA) developed by Fulde et al.^{30–39} has been found to be quite successful in describing the band structure of semiconductors and insulators. In this way, Horsch et al.⁴⁰ developed the general theory of the LHA (also referred to as projection technique) in which the total Hamiltonian is projected in a model space containing the eigenstates of the $N \pm 1$ system dominated by single-particle configurations; Later, Stoll³¹ introduced an ab initio treatment based on local HF orbitals by creating an incremental scheme of correlation contributions to the ground-state energy⁴¹ which was extended to deal with QP excitations^{32,33} and applied to the valence bands of covalent semiconductors.³⁴ The subsequent development of the so-called cluster-in-solid embedding technique³⁵ also allowed the correlated conduction band structure to be obtained.^{36,38,39} The latest results by applying this quantum-chemistry approach have been obtained for the strongly correlated close-lying spin states in 3d-based compounds^{37,42} and the band structure of zinc blende ZnS, focusing on the Zn 3d “semicore” states.⁴³ These first-principle approaches rely on a HF wave function as the zero-order approximation for the ground state. The nonorthogonal CI is further used to correlate the hopping matrix elements which, within a tight-binding model, can be interpreted as the charge-transfer probabilities between neighboring sites. This technique is well suited to our scheme for describing the charge transfer states arising from localized adsorbate–substrate interactions.⁵ As a natural extension of our previous approach for excited states of molecules adsorbed on metal oxide surfaces by using a classical (finite) cluster model,^{5,16} we will apply and briefly describe an optimized version of the cluster-in-solid embedding technique.³⁵ In this approach, the Wannier orbitals and Hartree–Fock (HF) periodic wave function are used to select a finite cluster that, in conjunction with a HF-type optimal embedding potential, reproduces the main characteristics of the extended system at the HF level. Hereafter, the simplest version of the frozen local hole (FLHA) method is employed to account for the correlation effects. The approach is implemented in an interface program between the latest versions of the CRYSTAL code and the MOLPRO electronic structure package. This implementation is applied here to the reconstruction of the HF band structure with the finite cluster approach and to the description of the TiO₂ correlated bands. To the best of our knowledge, this technique is applied for the first time to bulk TiO₂, a prototype of early transition metal oxide.

The next section provides an outline of the underlying theory. This is then followed by a brief description of methodological and computational aspects of the implementation in section III. The following three sections describe the application of this technique to reproduce (and correlate) the periodic (HF) band structure of TiO₂ with the finite cluster approach. Section VII closes with a discussion of future applications and extensions of the technique. Some additional details of the implementation and its application to TiO₂ are provided in the Supporting Information.

II. OUTLINE OF THE THEORY

In a periodic system the atomic orbital (AO) becomes a crystalline orbital (CO) and is now represented as a combination of: a discrete index *i* which labels the AOs of atoms within a unit shell and a continuous 3D index *k* spanning the Brillouin zone. The crystalline Fock matrix is diagonal in *k*; however the integrals defining this Fock matrix do contain the integration over the whole Brillouin zone. The eigenvalues of this Fock matrix, as a function of *k* are called bands. The corresponding eigenfunctions $\phi_{k\alpha}(r) = \exp(ikr)u_{k\alpha}(r)$ are the Bloch functions (BFs), with α numbering the discrete eigenvalues (bands) $\varepsilon_\alpha(k)$ for a given *k* and $u_{k\alpha}(r)$ the periodic functions. The Bloch functions are well-defined from a “physical” point of view; they properly describe the collective effects in extended systems. However, while Bloch functions are local in *k*-space, they are quasi-periodic in real space. Therefore, these functions are completely delocalized in real space and cannot be normalized in a usual sense. As a result, they have no easy “chemical” interpretation and are hard to use in order to describe local processes.

Moving toward a more chemical perspective, a transformation to Wannier functions⁴⁴ (WFs) ψ is performed. It can be done for a single band

$$\psi_{n\alpha}(r) = \frac{1}{\sqrt{\Omega}} \int_{BZ} d^3k \exp(-ikR_n) \phi_{k\alpha}(r) \quad (1)$$

where Ω is the volume of Brillouin zone, or for a group of bands

$$\psi_{n\alpha}(r) = \frac{1}{\sqrt{\Omega}} \sum_\beta \int_{BZ} d^3k A_{\alpha\beta}(k) \exp(-ikR_n) \phi_{k\beta}(r) \quad (2)$$

with $\hat{A}(k)$ as a unitary matrix. Thus, we substitute the infinite continuous index *k* in the Bloch function by an infinite discrete index *n* numbering the unit cells, with R_n being the lattice vector associated with unit cell *n*.

In general, for a well isolated band or group of bands, the resulting Wannier functions are rather compact. However, they still might not be perfectly localized. In addition, the definition of Wannier functions is clearly not unique, as we can multiply each Bloch function by an arbitrary periodic *k*-dependent phase factor. This arbitrariness can be used to produce maximally localized Wannier functions (see, e.g., ref 45). If the group of bands used in such a transformation has a well-defined atomic character, the proper localization procedure will result in atomic-like functions called localized WFs (LWFs) in a similar way as with molecular systems. This is implemented within the Wannier–Boys localization module of the CRYSTAL code.^{46,47} Alternatively, real-space approaches to the direct determination of Wannier functions have been developed by Shukla et al.⁴⁸

Some important properties of LWFs are that they are orthonormal with respect to an integration over the entire space

$$\langle \psi_{n\alpha} | \psi_{n'\beta} \rangle = \delta_{n,n'} \delta_{\alpha,\beta}$$

are mostly localized on a given unit cell R_n (or better on a given atom), and translationally invariant: The set of LWFs associated with a given unit cell *n* of the crystal can be brought into coincidence with that of the unit cell *n'* by shifting the functions by the lattice vector $R_{n'-n}$

$$\psi_{n'\alpha} = \hat{T}_{R_{n'-n}} \psi_{n\alpha} \quad (3)$$

where \hat{T}_R denotes the translation operator by a passive translation of *R*.

The total HF wave function is invariant under unitary transformations of occupied and virtual orbitals. Therefore, it can be shown^{32–34} that the band energies $\varepsilon_\alpha(k)$ can easily be recovered from LWFs as eigenvalues of a complex Hermitian *k*-dependent Hamiltonian matrix

$$H_{\alpha\beta}(k) = \sum_n \exp(ikR_n) \langle \psi_{0\alpha} | \hat{H} - E_0 | \psi_{n\beta} \rangle \quad (4)$$

where for the HF case the Hamiltonian operator \hat{H} is a crystalline Fock matrix, with E_0 being the ground-state HF energy of the neutral system. When $\psi_{0\alpha}$ and $\psi_{n\beta}$ are centered on the same atom, the matrix elements (MEs) $\langle \psi_{0\alpha} | \hat{H} | \psi_{n\beta} \rangle$ are called “on-site”, whereas the off-diagonal terms are denoted as “hopping” matrix elements. These $\langle \psi_{0\alpha} | \hat{H} | \psi_{n\beta} \rangle$ terms, representing the hopping of a quasi-particle from the state α in the central unit cell 0 to the state β in the unit cell *n*, are nonzero because the Fock matrix is no longer diagonal when changing to LWFs. The advantage of this representation is that it is of a “chemical” form. For well-localized LWFs, the hopping matrix elements decay rapidly with increasing distance and the summation in eq 4 is typically restricted to close neighbors of the central unit cell 0. The spatial symmetry properties become more transparent as well. Furthermore, as described below, the approximate correlated bands can be obtained from the complex Hamiltonian matrix of the same form, but with the LWF Hamiltonian matrix elements $\langle \psi_{0\alpha} | \hat{H} | \psi_{n\beta} \rangle$ replaced by their correlated counterparts (see, e.g., ref 39 and references therein). Taking advantage of the local character of this representation, it is clear that a finite cluster “truncation” of the extended system can be a good approach to evaluate and correlate each matrix element with some corrections to effectively account for missing contributions from the infinite periodic environment. As described in the following section, this is performed by resorting to the “molecular counterpart” of eq 4 through the cluster-in-solid embedding technique developed by Birkenheuer et al. and first reported in ref 35. As in a typical divide-and-conquer strategy, the finite cluster is selected according to the specific matrix element to be correlated.

Before finishing this section, we discuss the WFs localization in more detail. If the group of bands is well isolated, the localization presents no problem. This is nearly always true for core bands, and in most cases for valence bands too. For virtual bands however, the case of entangled bands is quite frequent, when bands having different character intersect at some points in the Brillouin zone (most often close to the $k = 0$ Γ -point). This can make proper localization impossible, unless special techniques are used (i.e., by using band disentanglement procedures^{49–52}) or more bands are included. We will address this point later on when considering the virtual Ti(3d) bands of TiO₂.

III. METHODOLOGICAL AND COMPUTATIONAL APPROACH

A. The Finite Cluster Approach. As mentioned above, to move from a periodic to a finite cluster description, we employed the cluster-in-solid embedding approach developed by Birkenheuer et al.^{35,53,54} and later applied, for instance, to the description of the correlated bands of MgO,³⁶ hydrogen fluoride chains³⁸ and boron nitride,³⁹ with a number of improvements and extensions that we describe later in this section.

As a first step, the localized orbitals are calculated for the periodic system, using the Wannier–Boys module of the CRYSTAL code.^{46,47} These Wannier functions are projected onto the set of AOs of a finite cluster cut C from the periodic system, providing a set of occupied and virtual cluster functions $|\tilde{w}_p\rangle$. This cluster is divided into an “active” region C_A and a “buffer” region C_B whose role is to assess an accurate representation of the tails of the Wannier functions centered on C_A . In this way, all the occupied Wannier orbitals centered on the sites in the active region enter into the subsequent post-HF calculations explicitly, whereas orbitals located in the buffer region are frozen. The periodic Fock matrix is also projected onto cluster AOs, denoted as $F_{\alpha\beta}^{\text{crys}}$. By using the set of occupied cluster functions $|\tilde{w}_i\rangle$, we can construct the occupied density matrix P^C and the corresponding Fock operator $F[P^C]$. The embedding potential is defined as the difference between crystalline and cluster Fock matrices

$$V_{\alpha\beta}^{\text{emb}} = F_{\alpha\beta}^{\text{crys}} - F[P^C]_{\alpha\beta}$$

This effective one-electron potential is added to the standard one-electron operator, followed by projecting out the unwanted orbital set,^{35,36} to reproduce the periodic environment. By itself, this is not sufficient and a proper projection of the frozen orbitals centered on C_B should be also performed. In practice, the quality of the embedding potential and the finite cluster approach itself can be checked by performing a closed-shell HF calculation for C (i.e., the energy and orbital relaxation should be very small for a good embedding potential and finite cluster C selection).

B. Computational Implementation. The original implementation of this approach⁵⁴ produces files which can be directly used by the standard quantum-chemistry package MOLPRO. The orbital projection algorithm is not implemented within MOLPRO; however, it can be easily emulated by adding the density matrix corresponding to the orbitals which must be projected out, to the one-electron Hamiltonian with a very big coefficient, e.g., 10^6 au. Since the energy minimum is searched for when performing HF and subsequent post-HF calculations, this procedure effectively projects out the unwanted orbitals (for details see section S1 of the Supporting Information).

For an efficient implementation of the approach, we optimized the original program as follows:

1. The original code was adapted to the latest available versions of both CRYSTAL09 (through the CRYAPI_OUT option) and MOLPRO 2010.1 programs packages.⁵⁵ Both codes contain important improvements over previous versions so that more complicated cases can be addressed. Furthermore, the original interface has been significantly rewritten and optimized to allow for larger cluster sizes to be routinely calculated.
2. The symmetry was implemented at the MOLPRO side of the code. Again, this will potentially allow for much larger systems to be calculated. Also, the explicit account for

spatial symmetry is important in many cases to avoid artificial symmetry breaking effects due to the N -particle space incompleteness of the computational methods used.

3. A special integral-direct code to evaluate nonsymmetric Fock matrices has been implemented using the development version of the MOLPRO package. Thus, by using an effective projection technique, it was possible to avoid the MCSCF/MRCI modules of the MOLPRO program in correlation calculations, which contain severe restrictions when applied to larger systems. This allowed us to treat much bigger finite clusters as compared to previous implementations.
4. An additional difficulty when treating the TiO₂ low-lying conduction bands is that, close to the Γ point, they are mixed up with higher bands making the localization of the Wannier functions difficult. Therefore, a special disentangling procedure has been devised (see section S4 of the Supporting Information).

C. Correlation Corrections to the Band Structure. As mentioned above, we used the quasi-particle formalism⁵⁶ and the local Hamiltonian approach^{32–34,38} to calculate the electronic correlation. The correlated matrix elements replace the Hartree–Fock ones in eq 4. These correlated matrix elements are obtained within the frozen local hole approximation (FLHA)^{36,37,39,56,57} as follows (we consider the valence bands as an example, the conduction bands are treated in a totally equivalent way):

1. For on-site matrix elements (we can assume that the Hamiltonian is diagonal on the subset of orbitals belonging to the same atom at the Hartree–Fock level, otherwise it can be readily diagonalized by orbital rotations), the hole is frozen for the target orbital and all other occupied orbitals are relaxed. In practice, this means that we perform an open-shell RHF calculation with a frozen single-occupied target orbital, frozen core and projection orbitals, and also by relaxing all occupied orbitals belonging to the active part C_A . This relaxation can be performed by shells of equidistant neighbors (to analyze the relaxation contribution as a function of the distance to the reference atom) and can be also classified according to the relaxed band. This correlation effect will be called on-site relaxation, and we explicitly account for it. Moreover, there are also long-range relaxation effects corresponding to the relaxation contributions summed over the infinite crystal. This is the so-called dielectric contribution which can be estimated through an empirical model whose quality is assessed by comparing with its ab initio counterpart calculated at intermediate range, as discussed below. Finally, we also take into account the loss of ground-state correlation coming from differential correlation effects due to the different number of electrons in the neutral and the ionic electron (hole) states; see below.
2. For off-diagonal hopping (corresponding to different atoms) matrix elements, two open-shell RHF states are constructed in a similar way (i.e., freezing a hole in the corresponding orbital and relaxing the rest) and the Hamiltonian matrix element is calculated over these two nonorthogonal RHF determinants.

It is worth stressing that, as demonstrated numerically and by the quasi-degenerate variational perturbation theory by Pahl and Birkenheuer,⁵⁷ the FLHA approximation provides an accurate description of electronic correlation that essentially corresponds

to the MRCI level of theory with single and double excitations. The simplified approach to the treatment used here (i.e., by resorting to self-consistent-field calculations with a ($N \mp 1$) single-state configuration where an electron has been removed (added) from (to) a localized occupied orbital) describes single-excitation correlation effects around a frozen local hole or electron. Since states beyond the one-particle excitation manifold are not considered, excitonic effects arising from the interaction between electron-addition and electron-removal states are not accounted for.

Compared to the implementations used in previous works,^{36,39} an important improvement was made to render the procedure more efficient and applicable to the much larger clusters needed to correctly describe the complicated TiO_2 band structure. Since in the RHF module of the MOLPRO code, used in finite cluster calculations, there is no possibility to freeze the core or the single-occupied hole orbital that is required in the FLHA approximation, the CASSCF module, which allows for freezing all required orbitals, was employed in refs 36 and 39 with a single configuration state function (CSF) as an equivalent of the ROHF determinant. However, for larger clusters when integral-direct calculations must be used, the CASSCF module is much less efficient compared to the RHF code that extensively employs the density-difference-based prescreening technique. By using the orbital projection possibility through the high-energy one-electron operator shift, as employed for the virtual orbital projection in the embedding potential itself, and by constructing effective one-electron operators through the MATROP module of MOLPRO, it was possible to apply the standard RHF code, thus making the calculations possible for larger cluster sizes. More details on the effective projection technique are given in section S1 of the Supporting Information.

As aforementioned, the correlation-corrected hopping matrix elements within the FLHA approach are obtained as the non-diagonal matrix elements of an effective Hamiltonian defined on the basis formed by two relaxed ROHF determinants. Since the relaxation is performed separately for the two involved holes (or electrons), the two ROHF determinants are built from mutually nonorthogonal orbital sets. Therefore, it is not possible to employ standard treatments to evaluate the transition matrix elements. In the previous implementations^{36,39} this problem was circumvented by employing a CASSCF one-determinant optimization followed by the MRCI module, which is used to cast the resulting ROHF determinant into MRCI format. In fact, the MOLPRO code has the possibility of evaluating transition matrix elements between MRCI wave functions built from different orbital sets.⁵⁸ This technique was already briefly described and applied in ref 5 and follows the method proposed by Malmqvist in ref 59, using a transformation to biorthogonal orbitals. However, this approach has technical limitations. First, the MCSCF module is much less efficient for large molecules (clusters) as compared to the ROHF code. Once again, the employment of the MCSCF module was necessary because it is not possible to freeze orbitals when the ROHF code is used. Second, the nonorthogonal transition module of MRCI is not implemented for integral-direct calculations, which are mandatory for the very large clusters used in this work. However, since in practice general MRCI states are not used but rather two simple RHF determinants with nonorthogonal orbitals, the corresponding hopping matrix elements are just the matrix elements of an effective nonsymmetric Fock matrix, which is calculated by using a nonsymmetric density matrix, as described

in section S2 of the Supporting Information. Therefore, a special integral-direct nonsymmetric Fock matrix routine was implemented within the development version of MOLPRO code which allowed us to calculate all the required hopping matrix elements even for clusters as large as $\text{Ti}_{52}\text{O}_{102}$.

Concerning the long-range dielectric relaxation, according to ref 56 (see p 207), the classical long-range polarization energy change due to an extra electron/hole is given in the continuum approximation by

$$\Delta E(R) - \Delta E(\infty) = \int_R^\infty d^3r \mathbf{P} \cdot \mathbf{E} = -\frac{\epsilon_0 - 1}{2\epsilon_0 R} \quad (5)$$

where \mathbf{P} is the electric polarization, \mathbf{E} is the electric (unscreened) field of the extra electron/hole, and ϵ_0 is the dielectric constant of the media, whereas $\Delta E(R)$ denotes the energy gain due to relaxation up to R . Actually, the expression in eq 5 is only valid for isotropic media, and not in the case of TiO_2 which, due to its anisotropy, has two different dielectric constants in directions both parallel and perpendicular to the c axis. However, a simpler approach was used here: By taking advantage of the fact that these dielectric constants are very large for TiO_2 , 124.74 and 96.28,⁶⁰ a simpler approximate expression was adopted

$$\Delta E(R) - \Delta E(\infty) \approx -\frac{1}{2R} \quad (6)$$

Within this classical approach, if we define the “external”, R_{ext} , and the “internal” R_{int} radii, associated to a given shell group as the average between the outer shell radius in the group and the radius of the next shell, the relaxation energy due to a given shell group would be given by

$$\Delta E = -\frac{1}{2} \left(\frac{1}{R_{\text{int}}} - \frac{1}{R_{\text{ext}}} \right) \quad (7)$$

Therefore, as mentioned below, when considering the correlation of the on-site matrix elements the accuracy of this approximation for long-range relaxation can be tested by computing the ab initio counterpart for the relaxation energy per shell group. In this way, as far as the classical estimate for a given group matches the ab initio value within a reasonable accuracy, we can safely apply eq 6 to get the relaxation energy for the rest of the crystal.

Finally, the loss of ground-state correlation (LGSC) due to the variation of the number of electrons in the hole (electron) states was estimated, following refs 36 and 39 but with a few differences:

1. In FLHA, the orbital corresponding to a given hole/electron state must be frozen. As MOLPRO does not provide a way to restrict excitations at CISD/MRCI levels, we proceed as follows: the hole/electron orbitals are frozen and all other on-site valence orbitals are relaxed. Then the full CISD method is applied to get the correlation energy. To account for overcounting of the correlation of the frozen orbital (the correlated wave function may contain configurations where the hole (electron) orbital occupation is not maintained), the double occupied valence orbitals are next frozen, whereas the single-occupied orbital is relaxed. In practice, it consists in diagonalizing the effective Fock operator (using the MATROP facility of MOLPRO). The single-occupied correlation energy is then calculated as the difference between the corresponding Fock matrix element and the Fock matrix eigenvalue. The difference between the

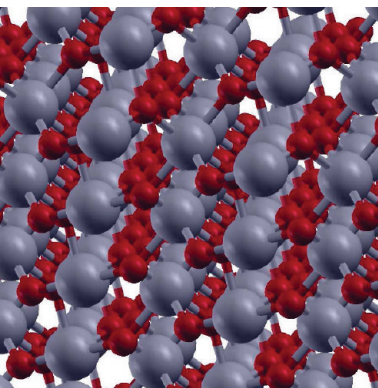


Figure 1. General view of the rutile TiO_2 bulk structure.

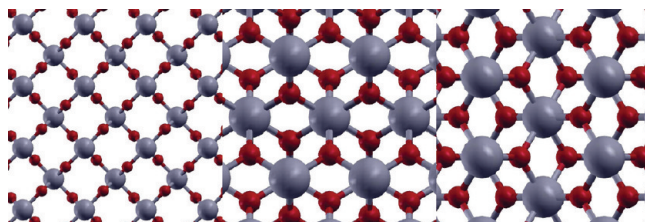


Figure 2. Z, X, and Y views of the rutile TiO_2 bulk crystal.

CISD correlation energy and the single-occupied orbital relaxation provides an effective CISD FLHA correlation energy. Further, an estimate of the LGSC is calculated as the difference between this energy and the ground-state CISD correlation energy.

2. In contrast to previous work^{36,39} the close lying virtual orbitals were found to be very important when correlating the on-site valence orbitals, especially for the O(2p) bands. Therefore, a larger active space was used—not just a single atom but including a few of the most important close lying metal neighbors. The neighbor orbitals are not correlated and are kept double occupied.

IV. BULK TiO_2 : STRUCTURE, DETAILS OF THE CALCULATIONS, AND SYMMETRY CONSIDERATIONS

Bulk TiO_2 (rutile) has a tetragonal unit cell with two formula units of TiO_2 . The space group is $D_{4h}^{14}\text{-P}4_2\text{/mnm}$ (No. 136). The crystalline orbital CRYSTAL09 code⁶¹ was used for all calculations. The cell parameters were fixed to their experimental values at room temperature:⁶² $a = 4.594 \text{ \AA}$, $c = 2.959 \text{ \AA}$, and $u = 0.306$. A high quality triple-valence all-electron atomic basis set was used and supplemented with additional *d*-symmetry functions on both titanium and oxygen atoms (Ti 86411(d41) and O 8411(d1)). This basis set was developed⁶³ and tested in detailed studies of bulk TiO_2 by Muscat et al. (for example see ref 64). The reciprocal space was sampled using a Monkhorst–Pack grid⁶⁵ with a shrinking factor subdividing the reciprocal lattice vectors (referred to as IS in ref 49) equal to 6. Tight thresholds for the integral calculations were used (the TOLINTEG parameters were set to 7, 7, 7, 7, 14, see the CRYSTAL manual⁶¹ for explanations) and the convergence accuracy for the total energies was set to 10^{-9} au . The real space lattice is shown in Figure 1, and the Cartesian sections are plotted in Figure 2.

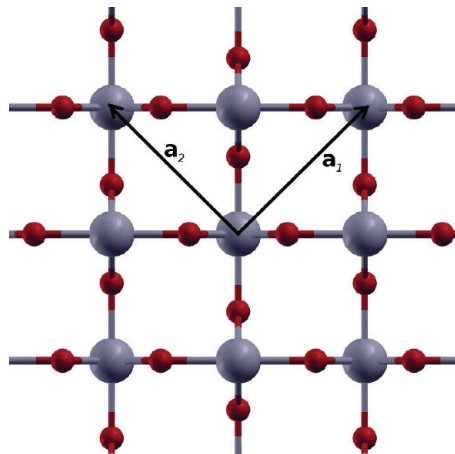


Figure 3. XY section view of the rotated crystal. The unit cell has twice the volume and a doubled atomic formula Ti_4O_8 . The original (nonrotated) cell vectors are also shown. This rotated crystal has an explicit D_{2h} x,y,z symmetry.

As clearly apparent in Figure 2, the whole lattice has D_{2h} point symmetry when placing the origin at Ti atoms or in the middle between two close oxygen atoms. This symmetry with the proper finite cluster selection (see next section) could be further used in MOLPRO calculations to noticeably reduce computing time and to explicitly account for symmetry properties. However, the D_{2h} group as implemented within the MOLPRO program, assumes the principal axes to be in the *x*, *y*, and *z* directions, which is different from the crystallographic standard as implemented in the CRYSTAL code. To deal with this problem, the whole crystal was rotated by 45° in the XY plane. This requires the use of a supercell with twice the volume and a cell parameter larger by a factor of $\sqrt{2}$. The space group is thus changed to $P4_2/n$ (No. 86) with $a = 6.497 \text{ \AA}$. The unit cell formula is therefore Ti_4O_8 . The XY section of such a grid is shown in Figure 3 where the original translation vectors \mathbf{a}_1 and \mathbf{a}_2 are also indicated.

The global TiO_2 band structure at HF level is presented in Figure 4 where the core $\text{Ti}(1s,2s,2p)$ and $\text{O}(1s)$ bands were omitted. In addition to the main symmetry directions in the \mathbf{k} space, the band structure along the directions $M \leftarrow R$ and $\Gamma \leftarrow A \leftarrow R$ of the Brillouin zone is also displayed. As seen below, this was necessary in order to fit some parameters corresponding to the 3d bands. The electronic band gap obtained at HF level, corresponding to the difference between the valence band maximum and the conduction band minimum, is 12.06 eV, greatly overestimating the experimental values derived from ultraviolet photoemission (UPS) and inverse photoemission spectroscopy (IPES) in rutile bulk (3.3 ± 0.5 eV)⁶⁶ and, more recently, in the $\text{TiO}_2(110)$ surface (3.6 ± 0.2 eV).⁶⁷ This can be compared with the DFT value (using the BLYP functional) of 1.90 eV. This value can be corrected by incorporating a fraction of single-determinant exchange within the hybrid DFT/HF approach.²⁶ Accordingly, a band gap of 3.62 eV with the B3LYP hybrid functional is obtained (containing a 20% of single-determinant exchange). Also very recent post-DFT GW studies^{68,69} predict electronic band gap values (3.59 and 3.34 eV) quite close to the experimental ones. On the other hand, the discrepancies of the details for the band dispersions are less pronounced. The calculated valence band

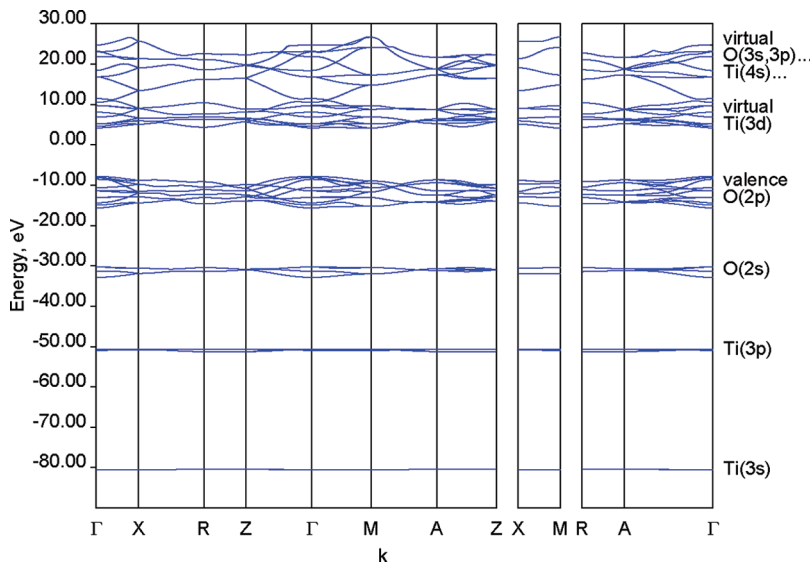


Figure 4. Global view of TiO_2 bands at HF level of theory. The entanglement between the highest $\text{Ti}(3\text{d})$ and the higher lying virtual band can be clearly appreciated.

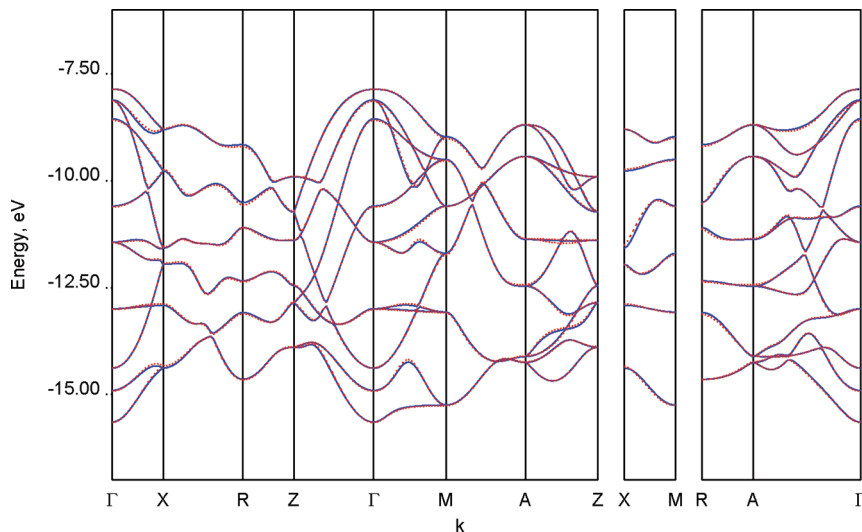


Figure 5. Valence $\text{O}(2\text{p})$ bands of TiO_2 calculated at Hartree-Fock level and modeled using a $\text{Ti}_{52}\text{O}_{102}$ cluster: solid blue, periodic CRYSTAL HF bands; red dashed, model bands with fitted interface-produced parameters.

widths at HF/B3LYP levels (7.79 and 6.30 eV) are somewhat overestimated as compared to the range of experimental values (5–6 eV⁷⁰).

V. RECOVERING THE HARTREE-FOCK BAND STRUCTURE WITH THE FINITE CLUSTER APPROACH

A. Valence $\text{O}(2\text{p})$ Bands of Bulk TiO_2 . The valence $\text{O}(2\text{p})$ bands of TiO_2 are well separated from both the lower lying $\text{O}(2\text{s})$ bands, and from the conduction $\text{Ti}(3\text{d})$ bands (see Figure 4). Therefore, their localization does not cause any special problem. The bands are depicted in Figure 5 (for modeled bands see below). In the upper panel of Figure 6 the corresponding LWFs are shown, as produced by the CRYSTAL code, and in the lower panel after the relocalization using a Pipek-Mezey AO transformation,⁷¹ as implemented in the MOLPRO code. It can

be noticed that the AO relocalization does not have any additional effect on the Wannier functions.

In order to build the $\text{O}(2\text{p})$ valence bands of TiO_2 within the finite cluster approach, a $\text{Ti}_{52}\text{O}_{102}$ cluster was used. A general view of this cluster as well as its projection on Cartesian planes is represented in Figure 7. To verify that this cluster size is large enough for an accurate treatment of the periodic HF problem, the HF relaxation energy was calculated by considering a $\text{O}_2\text{Ti}_4\text{O}_{12}$ cluster as the active C_A part, which is also shown in Figure 7. After relaxing the oxygen 2s and 2p orbitals and titanium 3s and 3p orbitals (the remaining orbitals were frozen), a relaxation energy value of only -0.00205 au was obtained, demonstrating that the cluster is properly selected and that the embedding potential is well-defined.

To extract the crystalline Fock matrix elements, the whole $\text{Ti}_{52}\text{O}_{102}$ cluster was used as the active part. Obviously, only

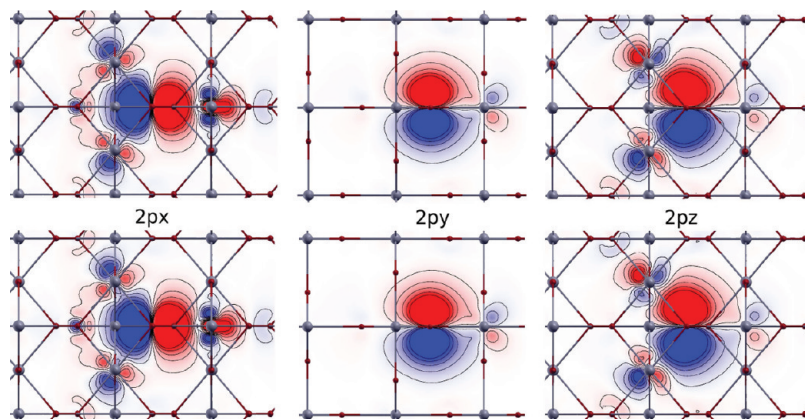


Figure 6. LWFs of oxygen 2p bands: upper panel, localized by the Wannier–Boys module of the CRYSTAL program; lower panel, after additional relocalization with the Pipek–Mezey LOCAO module of the MOLPRO code.

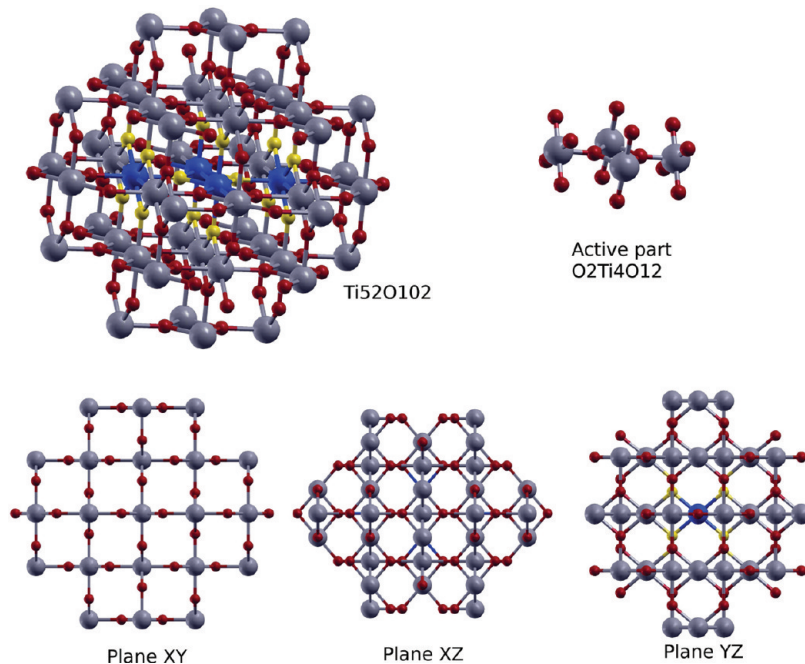


Figure 7. $\text{Ti}_{52}\text{O}_{102}$ cluster and active Ti_4O_{14} part used to model the valence (2p) bands of TiO_2 .

oxygen centers (with 2p-like orbitals on them) contribute to the reconstruction of the 2p bands, reflecting the Fock matrix structure and the symmetry relations between its elements. Clearly, titanium atoms also participate in the bands construction, which is manifested through the LWF hybridization during the Wannier localization in the direction of the close lying Ti atoms, as apparent in Figure 6. Therefore, the Fock matrix structure reflects the structure of an oxygen-only grid. In principle, all oxygen atoms in a periodic crystal are symmetry equivalent. Choosing one oxygen atom as the reference one (N_0), the Hamiltonian matrix elements are then classified by the orbital type (x , y , and z) and the neighbor centers, which are ordered according to the distance from N_0 . The closest oxygen atom is denoted as N_1 , the next one as N_2 , etc.; see Figure 8 where the oxygen grid is shown (only the neighbors having $z = 0$ or $z = c/2$ are displayed). Regarding the selected central oxygen site N_0 , it can be noticed that the oxygen atoms can be divided in

two categories: those lying on the same XY plane as N_0 (and all atoms obtained by an integer Z -translation), and those shifted by $c/2$ in the Z direction. The former atoms are highlighted in red and the latter in blue. By inspecting the Hamiltonian matrix elements and choosing only those larger than 0.0002 au, it can be demonstrated that only the subset of selected contributions from N_0 to N_{17} is important. More details about structural and symmetry relations are provided in section S3 of Supporting Information. The most important (larger than 0.005 au) matrix elements are listed in Table 1. The representative atoms of the i th shell of neighbors used to define the matrix elements are indicated explicitly in Figure 8 (see also section S3 of Supporting Information).

On the whole, the Hamiltonian model contains 60 independent symmetry terms. The results of this model are summarized above in Figure 5. It can be clearly seen that the valence band structure is perfectly reproduced. In particular, the value of the bandwidth is reproduced within 0.03 eV.

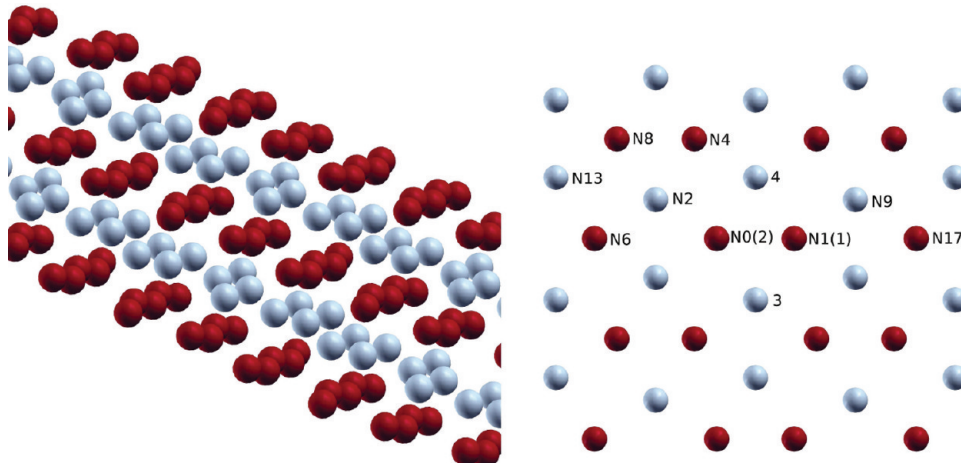


Figure 8. Oxygen grid demonstrating the structure of the 2p bands. For more information about the notation see section S3 of the Supporting Information.

**Table 1. Crystalline Fock Matrix Elements (MEs)
 $\langle \psi_{0\alpha} | \hat{H} | \psi_{n\beta} \rangle$ for Oxygen 2p Bands^a**

| shell | <i>i</i> | <i>j</i> | ME | fitted ME | ΔE_{corr} | final ME |
|--------------|-----------------|-----------------|-----------|-----------|-------------------|-----------|
| on-site (N0) | 2p _x | 2p _x | -0.457969 | -0.458379 | 0.121184 | -0.337196 |
| | 2p _y | 2p _y | -0.391023 | -0.390543 | 0.119343 | -0.271200 |
| | 2p _z | 2p _z | -0.437328 | -0.436719 | 0.120526 | -0.316193 |
| shell | <i>i</i> | <i>j</i> | ME | fitted ME | S_{corr} | final ME |
| N1 | 2p _x | 2p _x | 0.038127 | 0.038092 | 0.976905 | 0.037212 |
| | 2p _y | 2p _y | -0.011476 | -0.013787 | 1.019352 | -0.014054 |
| | 2p _z | 2p _z | 0.007923 | 0.007949 | 0.998725 | 0.007939 |
| N2 | 2p _z | 2p _x | -0.017003 | -0.017345 | 1.008060 | -0.017485 |
| | 2p _y | 2p _x | -0.015434 | -0.015159 | 1.014737 | -0.015382 |
| | 2p _x | 2p _x | 0.012330 | 0.012768 | 0.972904 | 0.012422 |
| | 2p _y | 2p _z | 0.007608 | 0.007024 | 0.972743 | 0.006833 |
| | 2p _z | 2p _y | 0.006625 | 0.006459 | 0.977747 | 0.006315 |
| N3 | 2p _x | 2p _z | -0.009321 | -0.008619 | 1.027507 | -0.008856 |
| | 2p _z | 2p _z | 0.010598 | 0.010587 | 0.970254 | 0.010272 |
| N4 | 2p _y | 2p _y | 0.008127 | 0.008253 | 1.000837 | 0.008260 |
| N5 | 2p _x | 2p _x | 0.017142 | 0.016749 | 0.963665 | 0.016140 |
| | 2p _y | 2p _y | 0.007531 | 0.007240 | 1.015352 | 0.007351 |
| | 2p _z | 2p _z | 0.024848 | 0.024452 | 0.966805 | 0.023640 |
| | 2p _x | 2p _z | 0.014541 | 0.014327 | 0.941388 | 0.013487 |
| N6 | 2p _x | 2p _x | 0.030730 | 0.030708 | 0.9666720 | 0.029686 |
| | 2p _y | 2p _y | 0.005003 | 0.008039 | 1.021716 | 0.008214 |

^a Only hopping (off-diagonal) MEs larger than 0.005 au are listed. Correlation corrections to the on-site and hoppings MEs are also given in the fifth and sixth columns. Positive corrections in ΔE_{corr} indicate an upward shift of the valence bands. For notations see text and section S3 of the Supporting Information.

B. Conduction Ti(3d) Bands of Bulk TiO₂. The localization of the virtual (conduction) bands often presents additional difficulties as compared to the valence bands, and the separation of LWFs that have a well-defined atomic character is quite involved. This is caused by the fact that the atomic-type bands, well identified and separated at some k-space points, may change the order at other points (especially at the high symmetry Γ point), with avoided crossings in the middle. This makes it

impossible to use straightforward band localization and it is thus necessary to apply some kind of disentangling procedure. This normally leads to an orbital with a well-defined character, but with energies (bands) different from the original HF values, which is in some way similar to a diabatization procedure in quantum chemistry approaches for molecular systems. A well-defined disentanglement procedure providing maximally localized Wannier functions has been proposed by Souza, Marzari, and Vanderbilt⁴⁹ and implemented, e.g., in the Wannier90 program package.⁷² The basic idea consists in using the energy window where the Bloch functions of different band groups are not intermixed. Recently, a similar procedure⁵¹ was implemented in the development version of the CRYSTAL code, but this is still not available in the official version.

The entanglement of the TiO₂ bands can be clearly seen in Figure 4 as an avoided crossing between the energetically highest Ti(3d) band and with the higher lying groups Ti(4s, ...) and O(3s,3p, ...). Fortunately however, the Wannier–Boys localization of the CRYSTAL code did converge and produced well-expressed Ti(3d)-type orbitals. The resulting LWFs corresponding to Ti(3d) bands are shown in the upper panel of Figure 9. We note that these plots might be a bit misleading as the plane sections are presented. In fact, though the grid has a well-defined D_{2h} symmetry, the orbitals do not. Actually, they do not lie in any symmetry plane and are instead localized along the main bonds. In this way, the first orbitals, have indeed an xy character, the two orbitals indicated as xz - and yz -type are actually a linear combination of those, and the last two orbitals (fully symmetric) have a (no pure) $z^2 - y^2$ and $2z^2 - x^2 - y^2$ (d_0) character.

To model the bands, the same Ti₅₂O₁₀₂ cluster as for the O(2p) bands, rotated 90°, was used. The CRYSTAL LWFs, shown in Figure 9, have been projected onto this cluster. As can be clearly seen in the upper panel of Figure 9, the LWFs are indeed well localized on the corresponding Ti centers. Therefore, the structure and the symmetry of Ti(3d) bands, according to eq 4, should follow that of the grid of Ti atoms. Both a general view and a XY plane section of this grid are drawn in Figure 10.

If one selected (reference) Ti atom is located at the origin (denoted as N0), the whole grid will have D_{2h} symmetry. The matrix elements in eq 4 can then be classified according to the orbital type and neighbor shell number. Figure 10 clearly shows that two types of Ti atoms can be distinguished: those placed on

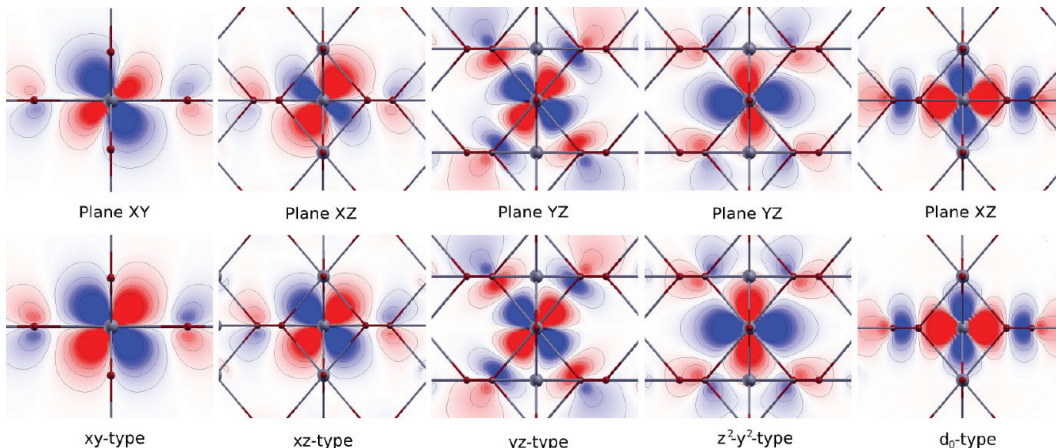


Figure 9. LWFs 3d. Upper panel: produced by CRYSTAL. Lower panel: final orbitals used to model the bands, after MOLPRO relocalization and additional rotation, as described in text.

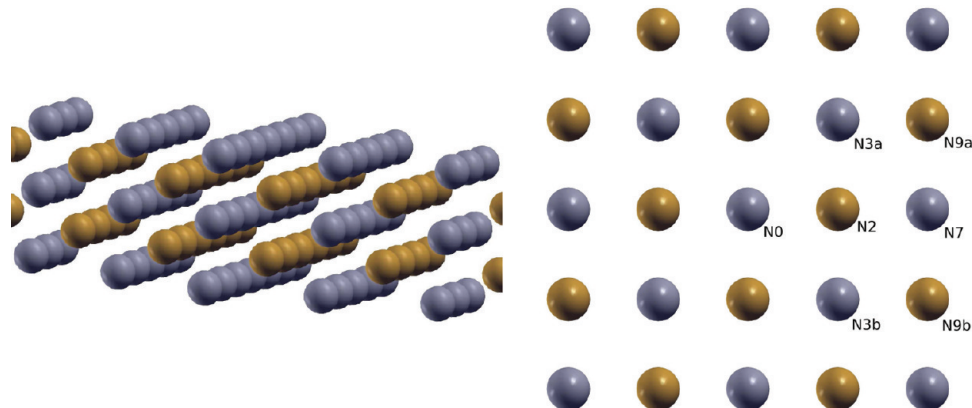


Figure 10. General view and XY section of the Ti-only grid, which defines the structure of Ti(3d) bands.

the same XY plane as $N0$ (and all atoms obtained by lattice translations along the Z axis), shown in gray, and those shifted by $c/2$ along the Z axis, highlighted in orange. Though the grid has D_{2h} symmetry, the X and Y directions are not equivalent due to the presence of oxygen atoms. It is noticeable however, that the lattice has a higher symmetry than a simple D_{2h} : the X direction on gray atoms is equivalent to the Y direction on orange atoms and vice versa. This imposes additional symmetry relations between the different Hamiltonian matrix elements. Though for Ti(3d) the corresponding generating spatial grid (Ti in this case) is rather simpler, of the body centered cubic type, there are additional complications as compared to the valence O(2p) bands. Indeed, if for O(2p) bands the CRYSTAL produces perfectly symmetry adapted LWFs, this is not the case for 3d bands, as can be clearly seen in Figure 9. In fact, the LWFs are localized mostly on important bonds and do not have proper D_{2h} symmetry. After postlocalization by MOLPRO using the Pipek-Mezey LOCAO module, these orbitals are further rotated and achieve perfect D_{2h} symmetry. However, while xy , xz , and yz type 3d orbitals are well-defined and have different symmetry properties, the situation is more complicated for x^2-y^2 and d_0 type orbitals. These orbitals have the same symmetry (fully symmetric) within the D_{2h} group, and hence they can rotate freely among themselves. Since actually the orbitals are not pure d orbitals but contain some (high) degree

of hybridization, there is no way to uniquely define them. This creates a problem when trying to model the bands, as the fitting procedure will contain one redundant parameter (i.e., the rotation angle) and will normally fail to converge. To deal with this problem, the rotation of these two orbitals was fixed by requiring that the corresponding off-diagonal crystalline Fock matrix element vanishes (all other off-diagonal on-site matrix elements are zero by symmetry). Additional details are provided in the Supporting Information. Final symmetry-adapted orbitals, which also correspond to the diagonal on-site crystalline Fock matrix, are shown in the lower panel of Figure 9. It can be noticed that the main effect of the MOLPRO postlocalization (i.e., the Pipek-Mezey transformation) is the rotation between xz and yz orbitals, and a sort of slight symmetry-adapting retouch of orbitals xy , z^2-y^2 , and d_0 .

By inspecting the Fock matrix elements in localized orbitals and selecting only matrix elements larger than 0.0002 au, it can be demonstrated that only a selected subset of contributions from neighbors $N0-N7$ and $N14$ is relevant.

As mentioned before, the Hamiltonian parameters were slightly adjusted to faithfully reproduce the HF bands. This is even more important for virtual bands, which are less localized as compared to the occupied bands leading to longer tails in the Fock matrix expansion. The disentanglement procedure is another point worth mentioning. In fact, the diagonal matrix

elements, as extracted from the CRYSTAL calculations, will reproduce some average energy of entangled bands, and therefore need to be adjusted. The reference energies used for the fitting also require special attention. Actually, the original bands are entangled so they cannot be employed as they are. An empirical disentangling procedure has been used, which is inspired by an electronic structure diabatization analogy, as described in detail in section S4 of the Supporting Information. On the whole, the effective Hamiltonian contained 61 terms. The terms that are larger than 0.005 au are listed in Table 2 (for orbital indices notations see the Supporting Information).

Table 2. Crystalline Fock Matrix Elements (MEs) $\langle \psi_{0\alpha} | \hat{H} | \psi_{n\beta} \rangle$ for Titanium 3d Bands^a

| shell | <i>i</i> | <i>j</i> | ME | fitted ME | ΔE_{corr} | final ME |
|-----------------------|----------|----------|-----------|-----------|--------------------------|-----------|
| on-site (<i>N</i> 0) | 1 | 1 | 0.221968 | 0.219933 | -0.188424 | 0.031509 |
| | 2 | 2 | 0.311706 | 0.312252 | -0.177182 | 0.134770 |
| | 3 | 3 | 0.223788 | 0.225475 | -0.187508 | 0.037967 |
| | 4 | 4 | 0.315967 | 0.316214 | -0.175228 | 0.140986 |
| | 5 | 5 | 0.223491 | 0.222996 | -0.188031 | 0.034965 |
| shell | <i>i</i> | <i>j</i> | ME | fitted ME | S_{corr} | final ME |
| <i>N</i> 1 | 1 | 1 | -0.012788 | -0.013203 | 0.684992 | -0.009044 |
| | 5 | 5 | 0.011965 | 0.012070 | 0.959618 | 0.011583 |
| | 1 | 2 | -0.015096 | -0.011053 | 1.047395 | -0.011577 |
| <i>N</i> 2 | 3 | 3 | 0.014913 | 0.015120 | 0.959059 | 0.014501 |
| | 2 | 1 | -0.016996 | -0.016215 | 1.018107 | -0.016509 |
| | 2 | 3 | -0.012630 | -0.013018 | 1.103512 | -0.014366 |
| | 5 | 4 | -0.010489 | -0.010566 | 0.974978 | -0.010302 |
| | 2 | 2 | 0.008599 | 0.009573 | 1.117860 | 0.010701 |
| | 5 | 5 | -0.007338 | -0.007366 | 1.022845 | -0.007534 |
| | 3 | 2 | -0.007775 | -0.008768 | 0.974405 | -0.008544 |

^aOnly hopping (off-diagonal) MEs larger than 0.005 au are listed. Correlation corrections to the on-site and hoppings MEs are also given in the fifth and sixth columns. Negative corrections in ΔE_{corr} indicate a downward shift of the conduction bands. For notations see text and section S4 of the Supporting Information.

The central result of this subsection is presented in Figure 11. Overall, it can be clearly seen that the finite cluster approach provides a 3d band structure that is hard to be distinguished from the one obtained with the periodic CRYSTAL code. In fact, the only difference is in the energetically highest 3d band that, within the finite cluster approach, becomes disentangled from the higher-lying group of bands. We also mention that the band gap is reproduced within 0.02 eV.

VI. CORRELATING THE TiO₂ BAND STRUCTURE

A. Correlation of the on-Site Hamiltonian Matrix Elements: 2p Valence Bands. To study the dielectric relaxation of the O(2p) valence bands, it was found that much larger cluster sizes are needed. The reason is that the relaxation energy converges much slower with the distance from the central atom as compared, for example, to the MgO and the zinc blende BN cases,^{36,39} reaching its asymptotic behavior only close to 10 au, which corresponds to the 19th neighbor of the hole oxygen atom and resulting in an active Ti₁₈O₄₄ cluster. Since the HF relaxation for the active part must be negligible as compared to the hole relaxation energy, the buffer zone must be large enough to ensure this small HF relaxation. In practice a 246 atom cluster Ti₈₅O₁₆₁ was used, which includes up to the 65th neighbor of the central oxygen. Fortunately, our current implementation allows treating such a large cluster size. Having relaxed the O(2s,2p) and Ti(3s,3p) orbitals, it was found that the relaxation of the Ti(3s,3p) orbitals becomes more important for atoms located at a long distance and is comparable with the relaxation of the O(2s,2p) orbitals, while being negligible for titanium atoms close to the central oxygen. First, the per-group shell relaxation of a selected O(2p_x) hole was studied. A summary of the results is presented in Table 3. For each group of shells, an “external” radius is defined as the average distance between the radius of the outer shell in the group and the radius of the next shell. For example, for group N1–N4 the external radius is calculated as an average of the fourth-shell radius ($R_4 = 5.2539$ au) and the fifth-shell radius ($R_5 = 5.5917$ au), thus giving $R_{\text{ext}} = 5.423$ au. Clearly, the approximation given by eq 7 may only work for shell groups that are far enough from the central atom. It was also found that

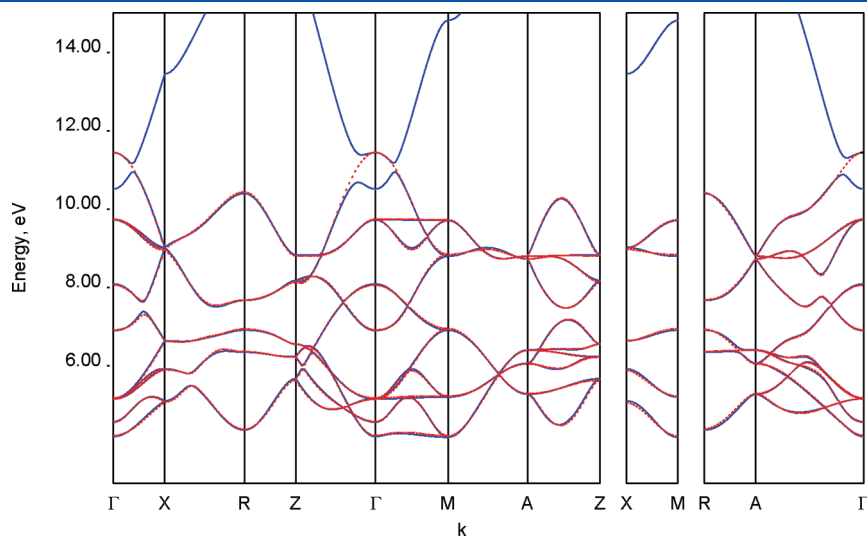


Figure 11. Conduction Ti(3d) bands of TiO₂ calculated at Hartree–Fock level and modeled using Ti₅₂O₁₀₂ cluster: solid blue, periodic CRYSTAL HF bands; red dashed, model with fitted interface-produced parameters.

Table 3. Relaxation of the Hole Located in the O(2p_x) Orbital

| shell group | group formula | R _{ext} , au | E _{relax} (hole), au | E _{relax} (HF), au | ΔE _{group} , au | ΔE _{classical} , au |
|------------------------------|----------------------------------|-----------------------|-------------------------------|-----------------------------|--------------------------|------------------------------|
| N0 | O | 1.836 | -0.079489 | -0.000003 | -0.079490 | |
| N1–N4 | Ti ₃ O ₉ | 5.423 | -0.127318 | -0.000011 | -0.047828 | |
| N5–N6 | O ₄ | 6.438 | -0.132541 | -0.000017 | -0.005224 | |
| N7–N10 | Ti ₄ O ₃ | 7.618 | -0.138319 | -0.000026 | -0.005778 | |
| N11–N12 | Ti ₄ O ₄ | 8.469 | -0.139594 | -0.000035 | -0.001275 | |
| N13–N15 | Ti ₅ O ₄ | 8.700 | -0.141083 | -0.000042 | -0.001490 | -0.00157 |
| N16–N17 | Ti ₂ O ₈ | 9.322 | -0.143467 | -0.000282 | -0.002384 | -0.00383 |
| N18–N19 | O ₁₀ | 9.843 | -0.146371 | -0.000793 | -0.002904 | -0.00284 |
| N0–N19 with Ti(2s,2p), O(1s) | Ti ₁₈ O ₄₄ | | -0.146389 | -0.000788 | | |
| N0–N19 | Ti ₁₈ O ₄₄ | | -0.146388 | -0.000789 | | |

the use of geometrical *S* factors as in refs 36 and 39 does not improve the agreement with the calculated relaxation energy. In any case, this *S*-factor is not used in the remaining long-range estimate. As mentioned above, the relaxation of the outer titanium orbitals is important at large distances. On the contrary, we have verified that the relaxation of the inner core orbitals is negligible, as is clearly apparent in Table 3.

The relaxation energy associated to a given atomic group shell is then defined as the energy difference between the relaxation energy summed over all the shells up to the outer one in the group and the relaxation energy without the atomic shells within the group in question. The shell relaxation energy itself is obtained by subtracting the neutral cluster (without the hole) relaxation using the same set of orbitals

$$\Delta E = E_{\text{relax}}(\text{hole}) - E_{\text{relax}}(\text{HF})$$

The corresponding values are also displayed in Table 3. This table clearly shows that, while for the inner shells E_{relax}(HF) is negligible as compared with E_{relax}(hole), it becomes relatively more significant for the outer ones. Still, for a selected large cluster and active part it can be considered as acceptable.

From Table 3 it can be seen that the agreement between the classical and the ab initio estimates becomes reasonable for the outermost shell group. Therefore, the long-range relaxation energy of the remaining infinite crystal can be estimated as

$$\Delta E_{\text{LR}} \approx -\frac{1}{2R_{\text{ext}}}$$

where R_{ext} is the external radius of the last explicitly considered group shell, i.e., the N18–N19 group, resulting in a value ΔE_{LR} of about -0.051 au.

Next, we consider the hole in the O(2p_y) and O(2p_z) orbitals. The fact that the relaxation energy becomes nearly independent of the hole type starting from the 19th neighbor, was checked. As an example, the relaxation energy due to the shell group N18–N19 is provided in Table 4. The use of an estimate for the long-range correlation energy which is independent of the hole type, is thus well justified. In Table 4 we also list the total relaxation energy due to shells N0–N19, and the total diagonal correlation corrections including the long-range term ΔE_{LR}, as well as the final correlated diagonal Hamiltonian matrix element, to be used for correlated bands calculations (see below). It is worth remembering that for hole correlation, this relaxation energy must be taken with a minus sign when correcting HF values.

Table 4. Correlation Corrections to the Diagonal Matrix Elements of the Valence O(2p) Bands^a

| | O(2p _x) | O(2p _y) | O(2p _z) |
|------------------------------------|---------------------|---------------------|---------------------|
| unfitted ME | -0.457969 | -0.391023 | -0.437328 |
| fitted ME | -0.458379 | -0.390543 | -0.436719 |
| ΔE _{corr} (N18–N19) | -0.002904 | | |
| ΔE _{corr} (N0–N19) | -0.146371 | -0.149614 | -0.147184 |
| ΔE _{LG} | | -0.050798 | |
| E _{corr} ^{CISD} | -0.157782 | -0.157656 | -0.157264 |
| E _{relax} ^{hole} | 0.039273 | 0.044231 | 0.040226 |
| ΔE _{LGSC} | 0.075985 | 0.081069 | 0.077456 |
| ΔE _{corr} | -0.121184 | -0.119343 | -0.120526 |
| final ME | -0.337196 | -0.271200 | -0.316193 |

^aNegative corrections in ΔE_{corr} indicate an upward shift of the valence band.

In order to account for LGSC, we used a Ti₁₁O₁₇ cluster with an active part C_A = Ti₃O. The O(2p_x) on-site relaxation using this cluster is -0.078290 au, which can be compared with the value of -0.079490 au obtained with the much bigger Ti₈₈O₁₆₁ cluster and active Ti₁₈O₄₄ part (see Table 3). The CISD correlation energy for the *N*-particle ground state (only the central oxygen 2s and 2p orbitals were correlated) equals to -0.194494 au. It is worth stressing here that by performing more advanced CCSD calculations, a quite close value for the ground-state correlation energy is obtained. In Table 4 the different contributions to the correlation energy from all valence O(2p) orbitals are shown together with the final value of the on-site matrix elements, including relaxation, the long-range polarization, and the LGSC. As can be seen in Table 4, the LGSC is practically independent of the valence orbital. Summarizing, on-site (short-range and long-range) relaxation effects leads to an upward shift of the valence band of ~5.4 eV while the loss of ground-state correlation yields an energy shift in the opposite direction and about half an order of magnitude smaller (~2.1 eV). These two corrections are thus partially compensated, giving an upward shift of ~3.3 eV. Within the framework of Green's function formalism and the self-energy approximation in the second-order perturbation theory, the relative importance of orbital relaxation and pure correlation contributions, as the LGSC correction, to the ionization energies of d transition-metal complexes was analyzed by Böhm.⁷³ Thus, it was shown that there is a clear interplay between the hybridization degree of the ligand orbitals where the hole "resides" and the relative weight of

Table 5. Relaxation of the $\text{Ti}(3d_{2y^2-x^2-z^2})$ Electron

| shell group | group formula | R_{ext} au | ΔE_{group} au | $\Delta E_{\text{classical}}$ au |
|-------------|---------------------------------|---------------------|------------------------------|----------------------------------|
| N0 | Ti | 2.7757 | -0.017656 | |
| N1 | O ₄ | 4.1946 | -0.087807 | |
| N2 | O ₂ | 5.3812 | -0.020024 | |
| N3–N6 | Ti ₁₀ O ₈ | 7.6770 | -0.008486 | -0.027786 |
| N7–N9 | O ₁₈ | 8.6801 | -0.007215 | -0.007527 |
| N10–N11 | Ti ₄ O ₄ | 9.8463 | -0.002564 | -0.006823 |
| N12–N13 | O ₈ | 10.3325 | -0.002856 | -0.002389 |

orbital relaxation and electronic correlation, with the latter being increasingly more important as the d metal character of the hole orbital increases. Despite the small hybridization degree of 2p LWFs with d metal orbitals, it is found that relaxation/polarization and LGSC corrections are of comparable magnitude. However, as emphasized by Birkenheuer and Pahl,³⁷ the orbital relaxations associated with a local hole is not the same as that corresponding to the electron vacant in a canonical HF orbital of the neutral system, the former comprising a bare electronic correlation at variance with the latter which is a pure mean-field correction arising from the breakdown of Koopmans' theorem in a finite system.

B. Correlation of the on-Site Hamiltonian Matrix Elements: 3d Conduction Bands and Comparison with the 2p Valence Bands. A similar cluster size is used here for the correlation corrections to the conduction (3d) bands: a Ti₇₇O₁₆₀ cluster centered on the correlated Ti atom, which includes up to the 40th neighbor of this central atom. The largest considered active part C_A, Ti₁₅O₄₄, contains up to its 13th neighbor and has an external radius of 10.333 au. The HF relaxation energy (including the O(2s,2p) and Ti(3s,3p) orbitals) with this active part is -0.00074 au. Once again, we found that the long-range correlation energy does not depend on the orbital and is well estimated by the empiric dielectric approximation; see Tables 5 and 6. To get final correlated values, both for valence and conduction bands, the correlation (explicit and long-range estimate) correction to the corresponding HF-fitted matrix element was added. In contrast with previous results obtained on MgO and BN crystals,^{36,39} it can be noticed that the differences between the total correlation correction for the different 3d orbitals is significant (up to 7% and more than 0.3 eV). Interestingly, despite the larger extent of the conduction-band 3d LWFs, longer-ranged correlation-induced effects were obtained for the local valence band 2p MEs.

In order to account for LGSC, a Ti₁₁O₁₄ cluster with an active TiO₆ part was used. The Ti(3d_{y²}) on-site relaxation of -0.017325 au can be compared with the value of -0.017656 using the much larger Ti₇₇O₁₆₀ cluster (see Table 5). The CISD ground-state correlation energy (only the central titanium 3s and 3p orbitals were correlated) is of -0.156073 au. This value differs by about 1.05 eV from that obtained for the 2p valence bands by using a Ti₁₁O₁₇ cluster with an active OTi₃ part (-0.194494). The orbitals that are correlated are different: doubled-occupied O-centered 2s and 2p orbitals (Ti-centered 3s and 3p orbitals) for the valence (conduction) bands, indicating the stronger correlation between the electrons in the former case. Table 6 displays the different contributions to the correlation of all the Ti(3d) orbitals. The LGSC contribution is rather small (at least by a factor of 7) compared to the valence O(2p) bands and it goes in the opposite direction (i.e., giving rise to an upward shift of the

Table 6. Correlation Corrections to the Diagonal Matrix Elements of Conduction Ti(3d) Bands^a

| | $d_{2y^2-x^2-z^2}$ | d_0 | d_{xz} | d_{yz} | d_{xy} |
|--|--------------------|-----------|-----------|-----------|-----------|
| unfitted HF | 0.221968 | 0.311706 | 0.223788 | 0.315967 | 0.223491 |
| fitted HF | 0.219933 | 0.312552 | 0.225475 | 0.316214 | 0.222996 |
| $\Delta E_{\text{corr}}(N0-N13)$ | -0.146606 | -0.139569 | -0.146494 | -0.133750 | -0.146567 |
| N12–N13 | -0.002856 | | | | |
| $\Delta E_{\text{corr}}^{\text{LG}}$ | | -0.048391 | | | |
| $E_{\text{corr}}^{\text{CISD}}$ | -0.150282 | -0.156147 | -0.149946 | -0.152048 | -0.150017 |
| $E_{\text{relax}}^{\text{hole}}$ | 0.000782 | 0.010251 | 0.001250 | 0.002888 | 0.000870 |
| $\Delta E_{\text{corr}}^{\text{LGSC}}$ | 0.006573 | 0.010178 | 0.007377 | 0.006913 | 0.006927 |
| ΔE_{corr} | -0.188424 | -0.177182 | -0.187508 | -0.175228 | -0.188031 |
| final ME | 0.031509 | 0.134770 | 0.037967 | 0.140986 | 0.034965 |

^aNegative corrections in ΔE_{corr} indicate a downward shift of the conduction bands.

conduction band). The absolute values (in the 0.18–0.28 eV range) are similar to those obtained for the conduction Mg-(3s,3p) band in bulk MgO;³⁶ however, the signs are opposite. In short, there is strictly no loss of ground-state correlation in the $N + 1$ states of bulk MgO. This behavior was explained by taking into account that the dominant correlation effect, when an electron is attached to a "formally" Mg²⁺ ion, is the polarization of the closed-shell core³⁶ since the ion has no valence electrons. It is well-known, however, that the reducible TiO₂ has an ionicity intermediate between ionic and covalent in contrast with the MgO case (a prototype ionic oxide) and that the charge of the Ti ion departs from the "nominal" 4+ value. Accordingly, LGSC corrections with the same sign were found for the conduction B(2s,2p) bands of the partially ionic boron–nitride.³⁹ Regardless what the compound is, the LGSC corrections are found smaller for the conduction band states. It is also worth noting that our estimate for correlation overcounting of the frozen hole (electron) is more than 3 times larger for hole-type states. Once again, the overcounting is due to the contribution of state configurations where the frozen (hole) electron occupation is altered in the correlated CISD ($N \pm 1$) wave function. As discussed in ref 39, the mixing with such configurations implies many-body effects beyond the QP picture which are experimentally mirrored as satellite peaks in the spectra.⁶⁶

On the whole, the downward shift of the 3d conduction-band due to on-site correlation effects roughly amounts to ~5.0 eV, which can be compared with the approximative estimate in the 2p valence band (3.3 eV). The averaged on-site short-range relaxation/polarization and long-range polarization contributions are almost equivalent in hole and electron states (4.0 vs 3.9 eV and 1.4 vs 1.3 eV, respectively). This is expected for a correlation contribution which can be interpreted as the polarization of the electronic cloud caused by the extra particle (of charge $\pm e$), confirming the accuracy of the adopted approach. In fact, this equivalence demonstrated that our results are converged with respect to the cluster sizes and associated active regions. In contrast, a large difference is found for the magnitude of the LGSC contribution (2.1 vs 0.3 eV). This is in line with results found for transition-metal-oxide complexes,⁷³ where small LGSC contributions were found for d metal-centered orbitals at variance with ligand molecular orbitals. The different physical nature of the LGSC contribution in $N - 1$ and $N + 1$ states can be understood in a somewhat simplified way, as follows: In anionic $N + 1$ states, the number of double-occupied orbitals is the same

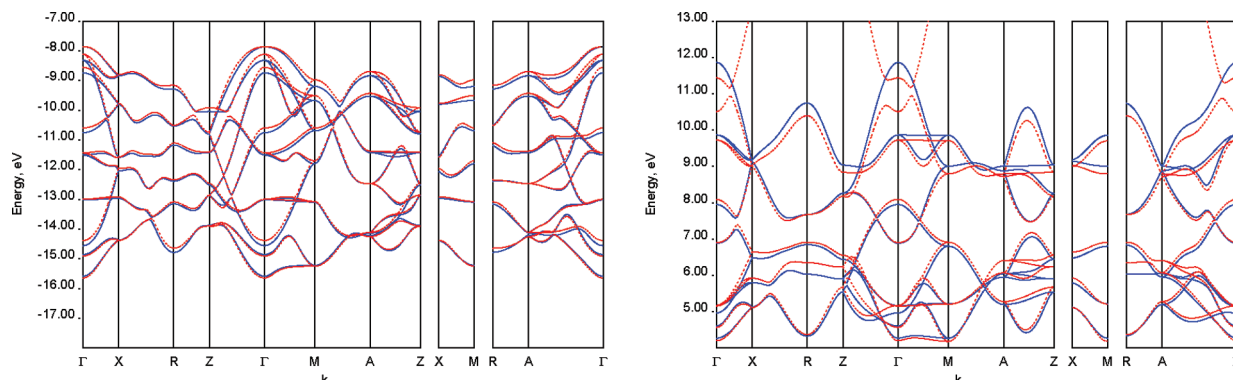


Figure 12. Valence O(2p) and conduction Ti(3d) bands of TiO_2 : solid blue, shifted correlated bands; red dashed, HF bands. The correlated bands are shifted so that their centers (average energy) coincide at the Γ point.

as in the ground-state. The missing part in a $N + 1$ FLHA state in comparison with the ground state is in the single/double excitations to the LUMO (no bonding) 3d orbital where the additional electron is located. The energy of the LUMO orbital is relatively high so that the amplitudes of these excited configurations in the wave function are small. In the case of cationic $N - 1$ states, the picture changes completely: the electrons located in valence HOMO (ligand) orbitals are strongly correlated with each other and the number of these electron pairs decreases for the hole $N - 1$ state. In particular, a large number of important virtual excitations experienced by these electrons to avoid each other are blocked when one HOMO orbital is occupied by a hole. Benchmark calculations on model systems by using the FLHA approach are necessary to get further insights into the key role of the LGSC contribution and other possible differential correlation effects.

C. Correlation of Hopping Matrix Elements. In order to correlate the hopping matrix elements, smaller cluster sizes were used. As the long-range contributions cancel out for hopping matrix elements due to orbital orthogonality,³⁶ this provides enough accuracy for these much smaller MEs. The selection of the cluster depends on the relative coordination of the two atoms that are involved. Both the full cluster and its active part should be symmetric with respect to these atoms. Starting with the O(2p) valence bands, it can be seen in Table 1 that only the N1–N6 neighbors of the central oxygen atom give hopping matrix elements larger than 0.005 au. Therefore, three different clusters were constructed: (a) a $\text{Ti}_{50}\text{O}_{102}$ cluster with an active Ti_6O_{29} part built on the three oxygen sites corresponding to the N0, N1, and N5 neighbors. This cluster is used to correlate the hopping MEs coming from N1, N3, and N5 neighbors (N1 and N5 are related as N0 and N3); (b) a $\text{Ti}_{45}\text{O}_{84}$ cluster with an active Ti_5O_{24} part built on N0 and N6 oxygen sites, this cluster is employed for N6 hoppings; and (c) a $\text{Ti}_{49}\text{O}_{94}$ cluster with an active Ti_7O_{27} part built on three (N0, N2, and N4) oxygen sites which is used for obtaining the remaining MEs.

Concerning the hopping matrix elements associated with the conduction Ti(3d) bands, only the N1 and N2 neighbors of the reference Ti atom make important contributions so that a different cluster for each of the two cases was used: a $\text{Ti}_{24}\text{O}_{80}$ cluster with an active Ti_2O_{10} part for correlating the N0–N1 hoppings, and a $\text{Ti}_{22}\text{O}_{78}$ cluster with $C_A = \text{Ti}_2\text{O}_{11}$ for the N0–N2 hoppings. To calculate the final (correlated) value of a given hopping matrix element, the following approach was used: from the relaxed calculation with the selected cluster, the scaling

factor $S_{\text{corr}} = H_{\text{LR}}^{\text{eff}}/H_{\text{LR}}^{\text{HF}}$ is evaluated (cf. eq 3 of the Supporting Information) as the ratio between the correlated and uncorrelated matrix elements, and the final value of the correlated hopping ME to be used for band calculations is obtained by multiplying the HF-fitted value $H_{\text{LR}}^{\text{HF,fit}}$ (Tables 1 and 2) by this scale factor. The pragmatic justification is that the fitting of hopping matrix elements effectively accounts for omitted long-range hoppings, which could be assumed to scale similarly. The difference between both fitted and selected cluster uncorrelated hopping ME values on one side and between correlated and uncorrelated hopping MEs on the other side is quite small in most cases (less than a few tens of millielectronvolts). Hence, this particular approach does not really affect the global result. Final values of correlated hoppings values are given in Tables 1 and 2.

From Table 1, it can be noticed that some hopping MEs associated with the valence (2p) bands are slightly increased and others are reduced by correlation corrections. The general trend is a reduction with the largest variation attained by the $2p_x$ – $2p_x$ intersite interactions with the N6 neighbor, about 0.03 eV. Corrections of similar magnitude were found for MgO and BN crystals albeit in the TiO_2 case these corrections are longer-ranged, affecting hoppings with rather distant neighbors (e.g., the N0–N6 MEs). As mentioned above, this is in contrast to the conduction (3d) hopping MEs where only N1 and N2 make a significant contribution. Similarly to the valence (2p) band case, some (3d) hopping MEs are enlarged and others are reduced (see Table 2). The largest correction (a reduction of about 0.11 eV and by a factor of 0.7) corresponds to the intersite hopping between $3d_{y^2-x^2-z^2}$ LWFs on the reference and the nearest-neighbor site. Somewhat smaller corrections were found for the anionic states of BN (0.06 eV as much) and MgO solids^{36,39} in contrast to the very significant reductions (up to a factor of 4) observed in more strongly correlated 3d compounds such as manganese oxide and cuprate crystals.^{74,75}

On the whole, correlation corrections to intersite hoppings between hole states are found to be much more long-ranged and smaller in magnitude than those obtained for the electron-states counterparts. Overall, the final (correlated) intersite hoppings are found larger and longer ranged for hole states, suggesting a higher probability transfer of photoexcited holes as compared with photoexcited electrons in the perfect crystal. At this stage, a comparison with previous results on the $\text{O}_2/\text{TiO}_{2-x}$ system⁵ can be made on a very qualitative basis. As compared with the ground state of the adsorbate–substrate complex, the lowest excited state roughly involves the charge transfer of an electron mainly

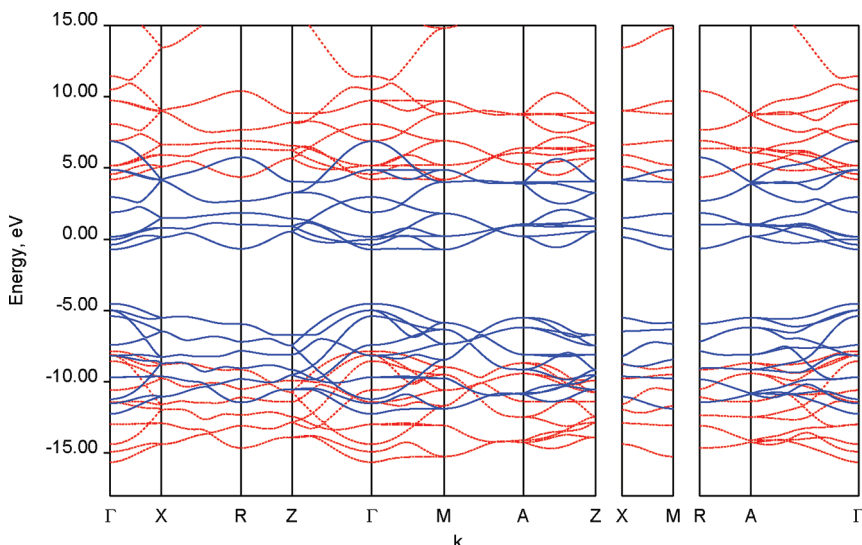


Figure 13. HF and correlated band structure of TiO_2 : solid blue, correlated bands; red dashed, HF bands.

located at an oxygen 2p-type orbital of the O_2 molecule (i.e., the oxygen atom oriented toward the surface) and the 3d orbital of a Ti atom located on the surface plane. At variance with the dipole-moment coupling, the electronic coupling between these two states was found to be quite small.⁵ It is for example 2 orders of magnitude smaller than the intersite hopping between the N0–N6 2p_x–2p_x hole states. Altogether, our results suggest a substrate-mediated photo-desorption mechanism through the “capture” of a photogenerated hole by the O_2 molecule in agreement with experimental findings.^{1,13–15}

D. Correlated Bands. The HF and correlated QP band structures are represented in Figure 13, whereas in Figure 12 the HF and correlated band dispersion are compared by putting into coincidence the average energy at Γ point of the corresponding 2p(3d) bands. Summarizing, short/range relaxation effects in bulk rutile TiO_2 are responsible for a reduction of the HF band gap by ~ 9.5 eV, which represents about 90% of the difference between the HF and experimental values. The long-range polarization caused by the extra hole or electron leads to an additional reduction of about 1.6 eV. The loss of ground-state correlation causes a lowering of the on-site MEs and a broadening of the band gap. The net effect of correlating on-site MEs is a reduction in the gap from 12.06 to 3.69 eV. The correlation of the off-site MEs causes an increase of the gap from 3.69 to 3.80 eV (the final value).

As is clearly apparent from Figure 12, in contrast to the large shift of the QP bands as compared with the HF counterpart, their shape (band-dispersion) is essentially unchanged. Only a very small narrowing (of around 0.06 eV) of the O(2p) valence band is obtained. It is worth stressing that the final computed band gap (3.80 eV) compares well with the UPS-IPES experimental values of 3.3 ± 0.5 eV⁶⁶ and 3.6 ± 0.2 eV.⁶⁷ The minimum energy difference between the valence and conduction bands is found at the Γ point. Experimental investigations⁷⁶ have determined that TiO_2 rutile is a direct-forbidden-gap semiconductor. Our results also indicate that the smallest “indirect” gap (along the Γ –M direction) is very close to the direct gap (within 0.015 eV). In the analysis of the optical absorption spectra, an indirect gap about

0.01 eV larger than the direct gap was estimated.⁷⁷ It is worth recalling, however, that the excitonic effects included in the optical spectra are not accounted for within the method.

VII. FINAL DISCUSSION: FUTURE PROSPECTS

A finite cluster approach³⁵ as well as our improvements and extensions have been described and illustrated in this paper through their application to the correlated band structure of a bulk TiO_2 crystal, as a prototype early 3d transition metal oxide. As far as we are aware, our work represents the first wave function based study of the band structure concerning a transition metal oxide. Summarizing, quasi-particle band structures obtained at a periodic HF level are almost perfectly reproduced by using the local cluster approach. The simplest version of the FLHA method (i.e., requiring just RHF calculations with frozen local hole or electron states) along with a dielectric approximation is then used to correlate the relevant on-site and off-site matrix elements within the local Hamiltonian approach. The inclusion of these correlation effects produced a very pronounced shift of the upper valence and lower conduction bands, the final band gap (3.80 eV) compares well with the experimental data (3.3 ± 0.5 and 3.6 ± 0.2 eV). In fact, the values of on-site effective Hamiltonian matrix elements are greatly affected by correlation effects. By comparison of correlation corrections for the on-site MEs of valence and conduction bands, it is found that on-site relaxation/polarization effects are rather similar, in contrast with the LGSC contribution which is about 7 times smaller in the latter case. On the other hand, off-site (hopping) matrix elements are much less affected by correlation effects. The correlation corrections of these values cause a small broadening (narrowing) of the band gap (valence bandwidth) by 0.11 eV (0.04 eV). In contrast with the band gap and similarly with previous studies on MgO and BN ^{36,39} the net effect on the included correlation effects on the valence bandwidth is very small. A narrowing of only 0.06 eV is obtained.

As future prospects, let us now discuss the applicability and possible advantages of using this approach to treat local effects. It is clear that in many cases local effects (e.g., point defects as oxygen vacancies, impurities and dopants in bulk materials and

on surfaces) need a multireference description. For example, many studies have shown the difficulty of a single-reference DFT or RHF/UHF level to properly describe oxygen vacancies in transition metal oxides, as reviewed in ref 78. Thus, the self-interaction error in DFT⁷⁹ is reflected in the electron delocalization of the excess charge from the oxygen vacancies of TiO₂ surfaces over many Ti sites, favoring a metallic solution instead of the localized defect states probed by the experiments.⁸⁰ In contrast, unrestricted HF calculations^{81,82} predict surface band gap states in TiO₂ which are insulating, but with the gap overestimated by about 9 eV (see above). A compromise was reached by either employing hybrid HF/DFT functionals or resorting to a DFT+U approach with the introduction of the so-called Hubbard *U* term for the on-site 3d repulsion.^{83–85} The main disadvantage of such approaches is their limited capability of prediction so that the degree of localization of the defect states depend either on the chosen value for *U*, that is then considered as an empirical parameter, or on the percentage of single-determinant exchange in hybrid HF/DFT treatments.⁸⁶ In short, the accuracy of these approaches is hard to be controlled systematically. In this regard, it is worth mentioning that a computational strategy based on an embedded cluster approach and multiconfigurational calculations has been devised to derive ab initio-based *U* values.⁸⁷

The difficulty in using a single-reference approach to describe, for example, oxygen vacancies can be easily understood by assuming that the removed oxygen is in its ground state, ³P, and that the “vacancy” state will have the same symmetry. Then it is clear that the description of a ³P state by a single-reference approach without introducing symmetry breaking effects (i.e., with an optimized structure at which a symmetry-broken solution becomes lower in energy than the symmetric solution) is problematic due to the selection of only one of the three degenerate components of the ³P state. In this case the molecular electronic-structure codes with a rich toolbox of correlated and multireference methods can be handy, provided the infinite periodic environment is properly accounted for.

In principle, the finite cluster approach can be easily extended to describe local defects with high level ab initio methods. Apart from the possibility of including correlation effects with well-proved wave function based methods in molecular systems, this approach offers obvious advantages over the standard supercell approximation when the local defect is isolated. Since the embedding potential is defined on all the AOs within the cluster C that mimics the bulk, the removal of one atom from its active part C_a and subsequent correlation of the wave function pose no additional problems. Thus, it would be interesting to analyze the influence of using either a HF approach or a multiconfigurational one for determining the charge distribution of the excess charge on different neighbor Ti sites to the oxygen vacancy in TiO₂, a matter in which there are still uncertainties (especially if these vacancies are located on the surface^{88,87–89}). However, in case of adding an extra excess atom (e.g., an interstitial Ti species in TiO₂) or considering a doping species replacing a lattice atom, the approach cannot be used “a posteriori” (i.e., on the defect-free cluster C) as the embedding potential is not defined on the new atom AOs. The same holds true for geometry relaxations as the “original” embedding potential is not defined on shifted AOs. A possible route to overcome this problem, provided the buffer region C_B is large enough, consists in simulating the (known) embedding potential on (known) AOs using, e.g., a large point-charge lattice with some fitted charges and/or positions. Then

this lattice, which effectively describes the environment, could be used on shifted/extraneous AOs. Another possibility is to use a pseudopotential lattice⁹⁰ which is a bit softer as compared to the point-charge-based embedding or combine it with the point-charge representation. Work along these lines is currently in progress. Similarly, the description of molecule/surface interactions in both ground and excited states by applying the computational approach at fixed adsorbate–surface geometries is also underway (i.e., to include dynamical correlation at the CC level). Recently, preliminary results were obtained to account for correlation effects in the interaction between a helium atom and the TiO₂(110) surface.⁹¹ Also, we find it interesting to check if the FLHA approach, in which only SCF calculations are necessary, is a cost-effective way of calculating the quasi-diabatic states and electronic couplings related to the ionic interaction of the adsorbate with the substrate, and to compare with the results obtained in our recent work on O₂/TiO_{2-x}.⁵ Following Hoffmann’s “local” view of extended systems,⁹² this work is another attempt at bridging the gap between traditional quantum chemistry and solid-state theory.

ASSOCIATED CONTENT

S Supporting Information. Information on (1) the projection technique, (2) the method to correlate off-diagonal matrix elements, (3) the valence and conduction bands, and (4) the empirical diabatization technique which has been used for the disentanglement between the energetically highest 3d bands. This material is available free of charge via the Internet at <http://pubs.acs.org>.

AUTHOR INFORMATION

Corresponding Author

*E-mail: Pilar.deLara.Castells@csic.es.

Notes

⁵E-mail: Alexander.Mitrushchenkov@univ-paris-est.fr.

ACKNOWLEDGMENT

This work has been supported by the CSIC-CM, MICINN-CSIC, and CM Spanish Grants Nos. CCG08-CSIC/ESP-3680, PIE.2007501004, and S2009-MAT-1467. The support of COST Action CM1002 (CODECS) is also acknowledged. A.O.M. acknowledges a fellowship from project No. PIE.2007501004. The calculations were performed at the Cesga SuperComputer Center (Galicia) and the computer centers at the UPEMLV and the Centro Técnico de Informática (CTI, CSIC). We warmly thank Uwe Birkenheuer, Hermann Stoll, and Peter Fulde for providing us access to the background CRYSTAL–MOLPRO interface in order to develop our computational implementation and Akbar Salam for suggestions on the manuscript. One of us (M.P.de.L.C.) thanks Carmela Valdemoro and Jeffrey L. Krause for their continued interest in this work.

REFERENCES

- (1) Yates, J. T., Jr. *Surf. Sci.* **2009**, *603*, 1605.
- (2) Lagunas, A. R. In *Abstracts of the 1st International Workshop on Molecular Photoreactivity on metal-oxide surfaces (FPMPMO-2009)*; de Lara-Castells, M. P., Aguirre, N. F., López-Durán, D., Mateo, J. O.,

- Mitrushchenkov, A. O., Eds.; Vision Netware: Madrid, 2009; pp 17, ISBN: 9788498868807.
- (3) Klüner, T. *Prog. Surf. Sci.* **2010**, *85*, 279.
 - (4) Mehdoui, I.; Klüner, T. *Phys. Rev. Lett.* **2007**, *98*, 037601.
 - (5) de Lara-Castells, M. P.; Mitrushchenkov, A. O.; Roncero, O.; Krause, J. L. *Isr. J. Chem.* **2005**, *45*, 59.
 - (6) Pisani, C.; Maschio, L.; Cassasa, S.; Halo, M.; Schütz, M.; Usvyat, D. *J. Comput. Chem.* **2008**, *29*, 2113.
 - (7) Hirata, S.; Podeszwa, R.; Tobita, M.; Bartlett, R. J. *J. Chem. Phys.* **2004**, *120*, 2581.
 - (8) Zhang, Z.; Yates, J. T., Jr. *J. Phys. Chem. Lett.* **2010**, *1*, 2185.
 - (9) Diebold, U. *Surf. Sci. Rep.* **2003**, *48*, 53.
 - (10) Thomson, T. L.; Yates, J. T., Jr. *Chem. Rev.* **2006**, *106*, 4428.
 - (11) Grätzel, M. *Nature* **2001**, *414*, 338.
 - (12) Henderson, M. A. *Surf. Sci. Rep.* **2011**, *66*, 185.
 - (13) Sporleder, D.; Wilson, D. P.; White, M. *J. Phys. Chem. C* **2009**, *113*, 13180.
 - (14) Zhang, Z.; Yates, J. T., Jr. *J. Phys. Chem. C* **2010**, *114*, 3098.
 - (15) Petrik, N. G.; Kimmel, G. A. *J. Phys. Chem. Lett.* **2010**, *1*, 2508.
 - (16) de Lara-Castells, M. P.; Krause, J. L. *J. Chem. Phys.* **2003**, *118*, 5098.
 - (17) Li, B.; Zhao, J.; Onda, K.; Jordan, K. D.; Yang, J.; Petek, H. *Science* **2006**, *311*, 1436.
 - (18) Doltsinis, N. L.; Marx, D. *Phys. Rev. Lett.* **2002**, *88*, 166402.
 - (19) Marques, M. A. L.; Gross, E. K. *Annu. Rev. Phys. Chem.* **2004**, *55*, 427.
 - (20) Duncan, W. R.; Prezhdo, O. V. *Annu. Rev. Phys. Chem.* **2007**, *58*, 143.
 - (21) Rego, L. G. C.; Batista, V. S. *J. Am. Chem. Soc.* **2003**, *125*, 7989.
 - (22) Wesolowski, T.; Warshell, A. *J. Phys. Chem.* **1993**, *97*, 8050.
 - (23) Huang, P.; Carter, E. A. *Annu. Rev. Phys. Chem.* **2008**, *59*, 261.
 - (24) Klüner, T.; Govind, N.; Wang, Y. A.; Carter, E. A. *Phys. Rev. Lett.* **2001**, *86*, 5954.
 - (25) Alkauskas, A.; Broqvist, P.; Pasquarello, A. *Phys. Rev. Lett.* **2008**, *101*, 046405.
 - (26) Islam, M. M.; Bredow, T.; Gerson, A. *Phys. Rev. B* **2007**, *76*, 045217.
 - (27) Hedin, L. *Phys. Rev.* **1965**, *139*, A796.
 - (28) Rinke, P.; Qteish, A.; Neugebauer, J.; Scheffler, M. *Phys. Status Solidi* **2008**, *245*, 929.
 - (29) Georges, A.; Kotliar, G.; Krauth, W.; Rozenberg, M. *Rev. Mod. Phys.* **1996**, *68*, 13.
 - (30) Fulde, P. *Adv. Phys.* **2002**, *51*, 909.
 - (31) Stoll, H. *Phys. Rev. B* **1992**, *46*, 6700.
 - (32) Gräfenstein, J.; Stoll, H.; Fulde, P. *Chem. Phys. Lett.* **1993**, *215*, 611.
 - (33) Gräfenstein, J.; Stoll, H.; Fulde, P. *Phys. Rev. B* **1997**, *55*, 13588.
 - (34) Albrecht, M.; Fulde, P.; Stoll, H. *Chem. Phys. Lett.* **2000**, *319*, 355.
 - (35) Birkenheuer, U.; Fulde, P.; Stoll, H. *Theor. Chem. Acc.* **2006**, *116*, 398.
 - (36) Hozoi, L.; Birkenheuer, U.; Fulde, P.; Mitrushchenkov, A.; Stoll, H. *Phys. Rev. B* **2007**, *76*, 085109.
 - (37) Hozoi, L.; Birkenheuer, U.; Stoll, H.; Fulde, P. *New J. Phys.* **2009**, *11*, 020323.
 - (38) Bezugly, V.; Albrecht, M.; Birkenheuer, U. *J. Phys.: Conf. Series* **2008**, *117*, 12006.
 - (39) Stoyanova, A.; Hozoi, L.; Fulde, P.; Stoll, H. *J. Chem. Phys.* **2009**, *131*, 044119.
 - (40) Horsch, S.; Horsch, P.; Fulde, P. *Phys. Rev. B* **1983**, *28*, 5977.
 - (41) Paulus, B. *Phys. Rep.* **2006**, *428*, 1.
 - (42) Hozoi, L.; Fulde, P. *Phys. Rev. Lett.* **2009**, *102*, 136405.
 - (43) Stoyanova, A.; Hozoi, L.; Fulde, P.; Stoll, H. *Phys. Rev. B* **2011**, *83*, 205119.
 - (44) Wannier, G. H. *Phys. Rev.* **1937**, *52*, 0191.
 - (45) Marzari, N.; Vanderbilt, D. *Phys. Rev. B* **1997**, *56*, 12847.
 - (46) Zicovich-Wilson, C. M.; Dovesi, R.; Saunders, V. R. *J. Chem. Phys.* **2001**, *115*, 9708.
 - (47) Baranek, B.; Zicovich-Wilson, C. M.; Roetti, C.; Orlando, R.; Dovesi, R. *Phys. Rev. B* **2001**, *64*, 125102.
 - (48) Shukla, A.; Dolg, M.; Fulde, P.; Stoll, H. *Phys. Rev. B* **1998**, *57*, 1471.
 - (49) Souza, I.; Marzari, N.; Vanderbilt, D. *Phys. Rev. B* **2002**, *65*, 035109.
 - (50) Thygesen, K. S.; Hansen, L. B.; Jacobsen, K. W. *Phys. Rev. Lett.* **2005**, *94*, 026405.
 - (51) Birkenheuer, U.; Izotov, D. *Phys. Rev. B* **2005**, *71*, 125116.
 - (52) Thygesen, K. S.; Hansen, L.; Jacobsen, K. W. *Phys. Rev. B* **2005**, *72*, 125119.
 - (53) Roetti, C.; Dovesi, R.; von Armin, M.; Alsheimer, W.; Birkenheuer, U. *The CRYSTAL-MOLPRO interface*, Max-Planck-Institut für Physik komplexer Systeme, Dresden, Germany.
 - (54) Birkenheuer, U.; Willmauer, C.; von Arnim, M.; Alsheimer, W.; Izotov, D. *scientific report*, Max-Planck-Institut für Physik komplexer Systeme, Dresden, 2002 (unpublished), Chapter II.1.8, p 71 (<http://www.pks.mpg.de/mpi-doc/quantum-chemistry/report18.html>).
 - (55) *MOLPRO, version 2010.1*, a package of ab initio programs designed by Werner, H.-J.; Knowles, P. J.; Lindh, R.; et al.; see <http://www.molpro.net>.
 - (56) Fulde, P. *Electron Correlations in Molecules and Solids*; Springer-Verlag: Berlin, 1995.
 - (57) Pahl, E.; Birkenheuer, U. *J. Chem. Phys.* **2006**, *124*, 214101.
 - (58) Mitrushchenkov, A.; Werner, H. *J. Mol. Phys.* **2007**, *105*, 1239.
 - (59) Malmqvist, P. A. *Int. J. Quantum Chem.* **1986**, *30*, 479.
 - (60) Rignanese, G.-M.; Rocquefelte, X.; Gonze, X.; Pasquarello, A. *Int. J. Quantum Chem.* **2005**, *101*, 793.
 - (61) Dovesi, R.; Saunders, V. R.; Roetti, C.; Orlando, R.; Zicovich-Wilson, C. M.; Pascale, F.; Civalleri, B.; Doll, K.; Harrison, N. M.; Bush, I. J.; D'Arco, P.; Llunell, M. *CRYSTAL09 User's Manual*, University of Torino, Torino, 2009.
 - (62) Rao, K. V. K.; Naidu, S.; Iyengar, L. *J. Am. Ceram. Soc.* **1970**, *53*, 124.
 - (63) Muscat, J. The phase stability, surface structure and defect chemistry of titanium dioxide from first principles techniques, *Ph.D. Thesis*, University of Manchester, Manchester, 1999.
 - (64) Muscat, J.; Swamy, V.; Harrison, N. M. *Phys. Rev. B* **2002**, *65*, 224112.
 - (65) Monkhorst, H. J.; Pack, J. D. *Phys. Rev. B* **1976**, *13*, 5188.
 - (66) Tezuka, Y.; Shin, S.; Ishii, T.; Ejima, T.; Suzuki, S.; Sato, S. *J. Phys. Soc. Jpn.* **1994**, *63*, 347.
 - (67) Rangan, S.; Katalinic, S.; Thorpe, R.; Bartynski, R. A.; Rochford, J.; Galoppini, E. *J. Phys. Chem. C* **2010**, *114*, 1139.
 - (68) Chiodo, L.; García-Lastra, J.; Iacomino, A.; Ossocini, S.; Zhao, J.; Petek, H.; Rubio, A. *Phys. Rev. B* **2010**, *82*, 045207.
 - (69) Kang, W.; Hybertsen, M. S. *Phys. Rev. B* **2010**, *82*, 195108.
 - (70) Woicik, J. C.; Nelson, E. J.; Kronik, L.; Jain, M.; Chelikowsky, J. R.; Heskett, D.; Berman, L. E.; Herman, G. S. *Phys. Rev. Lett.* **2002**, *89*, 077401.
 - (71) Pipek, J.; Mezey, P. G. *J. Chem. Phys.* **1989**, *90*, 4916.
 - (72) Mostofi, A. A.; Yates, J. R.; Lee, Y.-S.; Souza, I.; Vanderbilt, D.; Marzari, N. *Comput. Phys. Commun.* **2008**, *178*, 685.
 - (73) Böhm, M. C. *J. Phys. B: At. Mol. Phys.* **1984**, *17*, 3103.
 - (74) Stoyanova, A.; Sousa, C.; de Graaf, C.; Broer, R. *Int. J. Quantum Chem.* **2006**, *106*, 2444.
 - (75) Hozoi, L.; Laad, M.; Fulde, P. *Phys. Rev. B* **2008**, *78*, 165107.
 - (76) Amtout, A.; Leonelli, R. *Phys. Rev. B* **1995**, *51*, 6842.
 - (77) Pascual, J.; Camassel, J.; Mathieu, H. *Phys. Rev. Lett.* **1977**, *39*, 1490.
 - (78) Ganduglia-Pirovano, M. V.; Hofmann, A.; Sauer, J. *Surf. Sci. Rep.* **2007**, *62*, 219.
 - (79) Flores, F.; Ortega, J.; Vazquez, H. *Phys. Chem. Chem. Phys.* **2009**, *11*, 8658.
 - (80) Yim, C. M.; Pang, C. L.; Thornton, G. *Phys. Rev. Lett.* **2010**, *104*, 259704.
 - (81) de Lara-Castells, M. P.; Krause, J. L. *J. Chem. Phys.* **2001**, *115*, 4798.

- (82) de Lara-Castells, M. P.; Krause, J. L. *Chem. Phys. Lett.* **2002**, 354, 483.
- (83) Morgan, B. J.; Watson, G. W. *Surf. Sci.* **2007**, 601, 5034.
- (84) Morgan, B. J.; Watson, G. W. *J. Phys. Chem. C* **2010**, 114, 2321.
- (85) Stausholm-Møller, J.; Kristoffersen, H. H.; Himmemann, B.; Madsen, G. K. H.; Hammer, B. *J. Chem. Phys.* **2010**, 133, 144708.
- (86) Finazzi, E.; Di Valenti, C.; Pacchioni, G.; Selloni, A. *J. Chem. Phys.* **2008**, 129, 154113.
- (87) Calzado, C. J.; Hernández, N. G.; Sanz, J. F. *Phys. Rev. B* **2008**, 77, 045118.
- (88) Krüger, P.; Bourgeois, S.; Domenichini, B.; Magnan, H.; Chandresris, D.; Le Févre, P. L.; Flank, A. M.; Jupille, J.; Floreano, L.; Cossaro, A.; Verdini, A.; Morgante, A. *Phys. Rev. Lett.* **2008**, 100, 055501.
- (89) Minato, T.; Sainoo, Y.; Kim, Y.; Kato, H. S.; Aika, K.; Kawai, M.; Zhao, J.; Petek, H.; Huang, T.; He, W.; Wang, B.; Wang, Z.; Zhao, Y.; Yang, J.; Hou, J. G. *J. Chem. Phys.* **2009**, 130, 124502.
- (90) Barandirán, Z.; Seijo, L. *J. Chem. Phys.* **1988**, 89, 5739.
- (91) de Lara-Castells, M. P.; Aguirre, N. F.; Mitrushchenkov, A. O. *Chem. Phys.* **2011**; DOI: 10.1016/j.chemphys.2011.07.013.
- (92) Hoffmann, R. In *A Chemist's View of Bonding in Extended Systems*; Wiley-VCH: New York, 1988.